AMFORM, a new mass-based model for the calculation of the unit formula of amphiboles from Electron Micro-Probe analyses

FILIPPO RIDOLFI[1,*], ALBERTO ZANETTI[2], ALBERTO RENZULLI[3], DIEGO PERUGINI[4], FRANCOIS HOLTZ[1], ROBERTA OBERTI[2]

[1]Institut für Mineralogie, Leibniz Universität Hannover, 30167 Hannover, Germany

[2]CNR-Istituto di Geoscienze e Georisorse, Sede secondaria di Pavia, 27100 Pavia, Italy

[3]Dipartimento di Scienze Pure e Applicate, Università degli Studi di Urbino "Carlo Bo", 61029 Urbino, Italy

[4]Dipartimento di Fisica e Geologia, Università di Perugia, 06100 Perugia, Italy

ABSTRACT

In this work, we have studied the relationships between mass concentration and unit-formula of amphibole using 114 carefully selected high-quality experimental data, obtained by EMP (Electron Micro-Probe) + SREF (Single-crystal X-ray Structure REFinement) ± SIMS (Secondary-Ion Mass Spectrometry) analyses, of natural and synthetic Li-free monoclinic species belonging to the Ca and Na-Ca subgroups, and 75 Li-free and Mn-free *C2/m* end-members including oxo analogues of Ca amphiboles. Theoretical considerations and crystal-chemical driven regression analysis allowed us to obtain a number of equations which can be used to: (i) calculate from EMP analyses amphibole unit-formulae consistent with SREF±SIMS data, (ii) discard unreliable EMP analyses and (iii) estimate $^{W}O^{2-}$ and Fe^{3+} contents in Li-free *C2/m* amphiboles with relatively low Cl contents (≤1 wt%). The AMFORM approach mostly relies on the fact that while the cation mass in Cl-poor amphiboles

increases with the content of heavy elements, its anion mass maintains a nearly constant value, i.e., 22O + 2(OH, F, O), resulting in a very well-defined polynomial correlation between the molecular mass and the cation mass per gram ($R^2 = 0.998$).

The precision of estimating the amphibole formula (e.g., ^{T}Si±0.02, ^{C}Al±0.02, ^{A}(Ca+Na+K)±0.04 apfu) is 2-4 times higher than when using methods published following the last IMA recommended scheme (2012). It is worth noting that most methods using IMA1997 recommendations (e.g., PROBE-AMPH) give errors which are about twice those of IMA2012-based methods. A linear relation between $^{W}O^{2-}$ and the sum of ^{C}(Ti, Fe^{3+}) and ^{A}(Na+K) contents, useful to estimate the iron oxidation state of highly-oxidized amphiboles typical of post-magmatic processes, is also proposed. A step by step procedure (Appendix 1) and a user-friendly spreadsheet (AMFORM.xlsx, provided as supplementary material) allowing one to calculate amphibole unit-formulae from EMP analyses are presented. This work opens new perspectives on the unit-formula calculation of other minerals containing OH and structural vacancies (e.g., micas).

Keywords: Li-free amphiboles, oxo component, cation mass, amphibole oxidation, amphibole deprotonation, SREF, SIMS, Mössbauer spectroscopy

Corresponding author: filippo.ridolfi@uniurb.it

INTRODUCTION

Amphiboles are a supergroup of silicate minerals containing, either at the major- or at the trace-element level, most elements of geological/geochemical relevance (for a review, see Hawthorne et al. 2007). It has been largely recognized that the role of amphibole in understanding geological/planetary processes

and several health issues is of crucial importance (e.g., Forbes and Starmer 1974; Foley et al. 2002; Gunter et al. 2007; McCanta et al. 2008; Jackson et al. 2013; Smith 2014). Amphibole crystal-chemistry has captured the attention of many scientists over the years because of its intrinsic complexity (indeed, the term amphibole derives from the Greek "αμφιβολος", which means ambiguous; Haüy 1801; see also Cipriani et al. 2007) and its ability to record the steps of a wide range of geochemical and petrological processes due to a network of mutual relationships between cation ordering, chemistry of the associated phases (minerals and/or melt) and intrinsic parameters such as pressure, temperature and fugacity of volatile elements (Hammarstrom and Zen 1986; Holland and Blundy 1994; Al′meev et al. 2002; Oberti et al. 2000, 2007a; Ridolfi et al. 2010; Ridolfi and Renzulli 2012; Zhang et al. 2017). However, the prerequisite for using amphiboles as geological markers is the determination of their correct crystal-chemical formula (i.e., composition and site partitioning).

In the 70s and 80s, amphibole unit-formula calculation was a hot topic in the geological community (e.g., Stout 1972; Smith 1977; Leake 1978; Laird and Albee 1981; Hawthorne 1983; Rock and Leake 1984; Spear and Kimball 1984; Jacobson and Sorensen 1986) which has led to two major recommended schemes of the International Mineralogical Association (IMA; Leake et al. 1997; Hawthorne et al. 2012). Routine calculations of amphibole unit-formulae from electron microprobe (EMP) data may be seriously affected by inappropriate normalization procedures and/or the lack of accurate information on the oxidation state of iron and the contents of hydrogen and lithium (Leake et al. 1997; Al′meev et al. 2002; Hawthorne et al. 2012; Locock 2014). In particular, most of the published schemes for formula calculation do not account for the occurrence of O^{2-} as W anion (e.g., Tindle and Webb 1994; Leake et al. 1997; Al′meev et al. 2002; Esawi 2004; Dale et al. 2005) which allows the number of total negative (and positive) charges to theoretically vary between 46 and 48 (Hawthorne et al. 2012). The spreadsheet of Locock (2014) can only account for a maximum content of O^{2-} in the W- sites ($^{W}O^{2-}$) equal to 2 times the total content of Ti in C, thus disregarding the

contribution of the oxidation of Fe to balance deprotonation. This lack of information leads to poorly constrained cation contents (mainly cation underestimations) and Fe^{3+}/Fe_{tot} estimates which, at the best, are averages between the maximum and minimum values (e.g., Leake et al. 1997). Nevertheless, there is a large amount of amphibole literature data reporting H, $^{W}O^{2-}$ and Fe^{3+}/Fe_{tot} measurements and/or accurate estimates (e.g., Robinson et al. 1997; Bottazzi et al. 1999; Oberti et al. 2000; Tiepolo et al. 2003; Adam et al. 2007; Oberti et al. 2007b; Uvarova et al. 2007; Perinelli et al. 2012; Della Ventura et al. 2014) that can be used to improve the existing methods to calculate amphibole unit-formulae.

In this work, we use high-quality literature data and end-member compositions to analyze the relation between elemental concentration (by mass) and stoichiometry in the amphibole supergroup and propose a new mass-based method to be applied only to EMP data, that allows identification of bad analyses and calculation of the correct unit-formula of Li-free (and Mn- and Cl-poor) *C*2/*m* amphiboles, with an uncertainty 2-4 times lower than that of recently published procedures (i.e., Hawthorne et al. 2012; Locock 2014). Tests of the most used formula calculation methods (Tindle and Webb 1994; Dale et al. 2005; Locock 2014) are also provided as supplementary material.

ESSENTIAL DEFINITIONS

Amphibole supergroup has the general formula $A_{0\text{-}1}B_2C_5T_8O_{22}W_2$ (Hawthorne et al. 2012). The amphiboles considered in this work are Li- and Mn^{3+}-free *C*2/*m* species and their group elements include: A = Na, K, Ca, □ (vacancy); B = Ca, Na, Mn^{2+}, Fe^{2+}, Mg; C = Mg, Ti, Fe^{2+}, Mn^{2+}, Cr, Ni, Zn, Al, Fe^{3+}; T = Si, Al, Ti; W = OH^-, F, Cl, O^{2-} (where Mn, Cr, Ni, Zn and Cl are minor components, ≤ 0.2 atoms per formula unit, apfu). Site-assignments and stoichiometric constraints for these amphiboles are provided in Table 1 while Table 2 reports the ideal formula and composition of 75 end-members.

Definitions needed to follow the text are provided below. Note that most of the calculations needed to obtain the defined parameters are reported in Appendix 1.

- *original composition*: concentrations expressed as wt% of the oxides (SiO_2, TiO_2, Al_2O_3, Cr_2O_3, FeO_{tot}, NiO, ZnO, MnO, MgO, CaO, Na_2O, K_2O) and halogens (F, Cl) in the amphibole, usually measured by EMP analyses;
- *TEO*: *Total Elements and Oxides* (also named re-calculated total), wt% sum of oxides (see previous definition) and halogens (F, Cl), minus FeO_{tot} (total iron content) and the oxygen atoms balancing F and Cl (i.e., $O^{F,Cl}$), plus Fe_2O_3, FeO and H_2O calculated from the unit-formula (Appendix 1), where calculated H_2O values correspond to those measured by Secondary-Ion Mass Spectrometry (hereafter SIMS) or estimated by Single-crystal X-ray Structure REFinement (hereafter SREF) by published equations relating the oxo component to the *M*(1)-*M*(2) distance (Oberti et al. 2007a; see following section and Supplement 1 for methods). Note that *TEO* values from original compositions generally deviate from ideality (100 wt%);
- *normalized composition*: concentrations expressed as wt% of the oxides and halogens (F, Cl) in amphibole calculated from any unit-formula to obtain a value of *TEO* equal to 100 wt% (e.g., Table 1 and http://webmineral.com for end-members);
- M_r *(g/mol)*: molecular mass corresponding to the sum of the apfu of all elements (Table 1) previously multiplied by their atomic mass (A_r), ;
- *cmpg*: cation mass per gram, i.e., $cmpg = 10^{-2}(Si + Ti + Al + Cr + Fe + Ni + Zn + Mn + Mg + Ca + Na + K)$, calculated from the original or normalized compositions, all elements in wt% (see Appendix 1 for calculation). Note that *cmpg* is a mass ratio and it thus corresponds to the total cation mass divided by the sum of the total cation and anion masses for normalized compositions;

- X_i: mass of element *i* divided by the total cation mass (see Appendix 1). Note that X_i values are the same in normalized and original compositions;
- ${}^{Y}i$: element or ion *i* in a generic group-sites Y, where Y can be T, C, B, A and W (Table 1). When superscript is not reported, *i* refers to the total amount of *i* in amphibole. To avoid misunderstanding the total amount of iron is expressed as Fe_{tot} (e.g., Table 1);
- *CR (apfu·g/mmol)*: correlation ratio between the sums of the apfu and *mmol/g* (millimole per gram) of all cation components, i.e. $CR = \frac{\sum Si \rightarrow K\ apfu}{\sum Si \rightarrow K\ \frac{mmol}{g}}$ (Table 1). Note that *CR* is ideally equal to the apfu·*g/mmol* value of any cation (e.g., $CR^{Si} = \frac{Si\ apfu}{Si\ mmol/g}$) or anion (e.g., $CR^{F} = \frac{F\ apfu}{F\ mmol/g}$). Once precisely determined (see below), it can be easily used to calculate the apfu of each element multiplying *CR* by the element concentration in *mmol/g* (see Appendix 1);
- *Δcharge*: deviation from electroneutrality in an amphibole unit-formula (i.e., positive – negative charge sums);
- *dC* and *dB*: deviation from 5 apfu and 2 apfu in the C- and B-group cations in the selected unit-ormulae, not admitted by the stoichiometric constraints (Table 1; see also section Selection criteria of the calibration dataset);
- ΔC: the amount of Fe^{2+}, Mn and/or Mg exceeding 5 apfu and thus considered as B-group cations in the calculated formula (Table 1; Appendix 1).

DATA SELECTION AND TECHNIQUES

Composition and petrogenesis of the investigated amphiboles

We have studied the relationships between concentration and unit-formula in Li-free and Mn, Cl-poor monoclinic amphiboles belonging to the Ca, Na-Ca subgroups (and some of their oxo analogues) using a dataset carefully selected from the literature and from the CNR-IGG (Consiglio Nazionale delle Ricerche-Istituto di Geoscienze e Georisorse) amphibole database available in Pavia; selection was done based on the availability of accurate EMP+SREF±SIMS analyses. The dataset contains 114 oxides-formula pairs with the largest possible geochemical and geological variability; the oxo-amphiboles considered are kaersutite, ferri-kaersutite, oxo-potassic-chromio-katophorite, oxo-potassic-taramite, Ti-rich oxo-sadanagaite, Ti-rich oxo-pargasite and Ti-rich oxo-ferri-pargasite (see AMFORM.xlsx in the supplementary material). Compositions belonging to the sodium amphiboles were excluded because they may contain minor to moderate amounts of Li (e.g., Hawthorne et al. 1993) which cannot be detected and measured by EMP analysis.

The dataset includes published concentration (wt%)-formula (apfu) pairs of both 61 synthetic (Oberti et al. 2000; Bottazzi et al. 1999; Tiepolo et al. 2000; 2003; Adam et al. 2007) and natural amphiboles which are typical of geologically relevant systems (gabbro, peridotite, lherzolite, kyanite-eclogite, marble, metasomatic/skarn-type deposit and several types of metavolcanic amphibolites) and coming from different world-wide localities (Oberti et al. 1995; Vannucci et al. 1995; Robinson et al. 1997; Oberti et al. 2007b; 2015; Uvarova et al. 2007; Perinelli et al. 2012; Della Ventura et al. 2014). 53 unpublished oxides-formula pairs come from the CNR-IGG database and include amphiboles from extrusive rocks, mantle ultramafic rocks (hornblendites, pyroxenites, peridotites), peridotitic and pegmatitic veins (for a list, cf. AMFORM.xlsx).

Sample characterization

All the unpublished amphiboles had been analyzed by EMP, SREF and SIMS allowing a complete characterization of their crystal-chemical parameters (AMFORM.xlsx). SREF and SIMS analyses were

158 done at CNR-IGG in Pavia, while EMP analyses were mostly done at the University of Manitoba
159 (Winnipeg, Canada). See electronic supplement 1 for a more detailed information on the CNR-IGG
160 analytical methods. The crystal-chemical formulae were calculated by combining SREF, EMP and
161 SIMS results. The number of A-cations was estimated on the basis of the refined site-scattering values
162 at the relevant sites and the K_2O and Na_2O contents from EMP analysis. The oxo component was
163 evaluated either by SIMS or by a SIMS-calibrated crystal-chemical relationship (Oberti et al. 2007a;
164 see also electronic supplement 1). Under these constraints, the Fe^{3+} content can be derived based on the
165 overall electroneutrality. The Fe^{3+} content and its distribution were further constrained through the
166 pattern of refined mean bond-lengths observed at the three *M*(1-3) octahedra. The presence of the *M*(4′)
167 subsite, indicating the occurrence of small B cations (i.e., Mn^{2+}, Fe^{2+}, Mg), was checked on the
168 difference Fourier maps. B cations were calculated assigning excess C cations (i.e., ΔC, first Mn^{2+} and
169 then Fe^{2+} and Mg) trying to minimize the difference between the site scattering calculated (from EMP)
170 for the B and C cations and those obtained by SREF. For further validation, the ^{T}Al contents obtained
171 by recalculation of EMP analyses was checked to be in close agreement with those calculated from the
172 refined <*T*(1)-O> and <*T*(2)-O> distances (Oberti et al. 2007a).

173 Many of the amphiboles taken from the literature include EMP, SREF and SIMS data, and their
174 formulae were obtained following the same procedure. The amphibole formula selected from Robinson
175 et al. (1997) was derived from EMP, SREF, Mössbauer spectroscopy (for Fe^{3+}/Fe_{tot}), wet-chemical (for
176 F) and IR (InfraRed spectroscopy, for H_2O) analyses. In some cases, the formulae were derived from
177 the only EMP and SREF data (Oberti et al. 1995; Vannucci et al. 1995; Oberti et al. 2007b; Della
178 Ventura et al. 2014), and the oxo component was estimated using the correlation developed at CNR-
179 IGG in Pavia based on SREF results (Oberti et al. 2007a). In other cases, the Fe^{3+} content of the
180 amphibole was validated by Mössbauer spectroscopy (Uvarova et al. 2007, Perinelli et al. 2012). For

181 the oldest selected data (Oberti et al. 1995) the occurrence of $^{W}O^{2-}$ in amphibole was estimated during
182 this work using the published SREF data (see above).
183
184 **Selection criteria of the calibration dataset**
185 Both literature and unpublished analyses were checked according to a series of criteria aimed at
186 obtaining a high-quality dataset.
187 Whenever standard deviations (oxide σ) of the EMP element oxide analyses are available
188 together with averaged compositions, we discarded amphibole data showing oxide σ values higher than
189 2/3 of the average oxide σ values reported by Ridolfi and Renzulli (2012) for their high-quality
190 experimental amphibole compositions. We also discarded the amphibole compositions with *TEO*
191 values falling outside the range of 100±1.7 wt%, because larger deviations from 100 wt% may derive
192 from analytical problems for some elements, resulting in error propagation to the unit-formula. The
193 amphibole compositions in the dataset have *TEO* values ranging from 98.3 to 100.8 wt%.
194 Amphibole formulae showing *Δcharge* larger than ±0.05, *dC* and *dB* larger than ±0.01 and/or
195 total cation apfu (i.e.,∑Si→K; Table 1) higher than 16.005 were also discarded. In addition, formulae
196 calculated without considering the oxo component, i.e., forcing the negative charges to be 46, were not
197 considered. The bijection between the composition and formula of any amphibole was carefully
198 checked comparing the *CR* values of each of the major elements (e.g., CR^{Si}, CR^{Al}, CR^{Mg}) with the *CR*
199 value calculated on the total cation sum (∑Si→K; Appendix 1). This procedure allowed us to avoid
200 mismatches between formulae and compositions due to adjustment and/or editing.
201 The dataset used to calibrate the method contains 114 entries and it is included in the
202 AMFORM.xlsx spreadsheet (provided as supplementary material). The ranges in elemental
203 composition are: ^{T}Si = 5.8-7.8 apfu; $^{A}(Ca+Na+K)$ = 0.1-1.0 apfu; $^{W}F \leq 1.3$ apfu; $^{W}Cl \leq 0.2$ apfu;
204 $Mg/(Mg+Fe^{2+})$ = 0.2-1.0; Fe^{3+}/Fe_{tot} = 0.0-1.0.

It is worth noting that oxides-formula pairs not validated by SREF were not included in this final calibration dataset. This decision was taken to guarantee an independent check of the formulae and a reliable constraint on ∑Si→K values.

Beside the 114 selected amphibole compositions, for calibration we used 75 ideal formulae and (normalized) compositions of Li- and Mn-free *C*2/*m* end-members of the amphibole supergroup (Hawthorne et al. 2012) (Table 2). The oxides-formula pairs in Table 1 also include kaersutite, ferri-kaersutite, ferro-kaersutite, ferro-ferri-kaersutite and some oxo analogues of the Ca groups as these amphiboles in nature may often have a significant oxo-component.

RATIONALE AND DATA ANALYSES

The high-quality dataset described above was used to detect and analyze any possible relation between compositional (e.g., wt% and *mmol/g*) and unit-fomula parameters (apfu) in amphiboles.

For a correct characterization of the amphibole unit-formula, two crucial parameters must be determined: ∑Si→K, ranging from 15 to 16 apfu and the oxo component ($^{W}O^{2-}$; 0-2 apfu), which allows the sum of the negative charges to vary between 46 and 48 (Table 1). When these parameters are known and the presence of Mn^{3+} can be excluded, the amount of Fe^{3+} can be derived under the constraint of electroneutrality (Hawthorne et al. 2012).

Development of the *CR*-equations

The correlation ratio (*CR*) between apfu and *mmol/g* of any component or sum of components (e.g., Si; Fe_{tot}, F; ∑Si→K) must be constant for any normalized and end-member composition-formula pair. If

226 *CR* is known with a reasonably good approximation, the apfu content of each element can be calculated
227 multiplying *CR* by its concentration in *mmol/g*.

228 Figure 1a shows that the *CR* of the normalized and end-member compositions is perfectly
229 correlated with their molecular mass, M_r:

230 $$CR = 10^{-3} M_r \ (apfu \cdot \frac{g}{mmol}) \qquad (R^2 = 1.000) \qquad (1)$$

231 Indeed, equation (1) is an identity because *CR* is mathematically equal to M_r divided 1000 for
232 the ideal composition of any mineral and compound. The original amphibole compositions only
233 slightly deviate from this linear trend (blue symbols in Fig. 1a). The deviations are due to *TEO* values
234 usually lower than 100% (see above). However, this simple correlation cannot be used to estimate *CR*
235 from EMP analysis because M_r can only be calculated from the formula. Indeed, equation (1) should be
236 used at the end of any formula calculation procedure to calculate *CR* after *Mr* has been calculated from
237 the formula, thus validating the final results and the quality of the data (see below).

238 Figure 1b shows that the *CR* values of normalized and end-member compositions have a nearly
239 perfect polynomial relation with the cation mass per gram (*cmpg*) which can be directly calculated
240 from EMP data (see above):

241 $$CR = 4.809 cmpg^2 - 3.409 cmpg + 1.276 \ \textit{(apfu·g/mmol)} \qquad (R^2 = 0.998) \qquad (2)$$

242 Indeed, the anion components in the different amphibole compositions have almost the same
243 mass, because they mostly consist of the same number of ions with similar A_r, i.e., $22O^{2-}$ +2(OH^-, F^-,
244 O^{2-}). In contrast, the mass of the cation component increases with the amount of heavier cations (e.g.,
245 Fe^{2+}, Fe^{3+}) resulting in a progressively increasing pattern of *CR* (and M_r) with *cmpg.* Because *cmpg* is a
246 mass ratio, Figure 1b has a curvilinear trend. The small scattering observed for some normalized and
247 end-member compositions (R^2 = 0.998; Fig. 1b) is due to the occurrence of $^W(Cl^-, F^-, O^{2-})$ which have
248 A_r values different from that of OH^-, thus affecting the *cmpg* values. For example, the heaviest end-
249 member ferro-ferri-cannilloite has the same cation mass as its oxo analogue but a higher M_r value

because it differs (in mass term) by having two more hydrogen atoms (Table 2). Therefore, the mass of W anions is higher than that of its oxo equivalent (because OH^- is heavier than O^{2-}) resulting in a *cmpg* value slightly lower than that of oxo-ferro-ferri-cannilloite (Fig. 1b; Table 1). F-rich amphiboles behave in the opposite way because F^- has a mass higher than OH^-. However the effect of F^- and $^{W}O^{2-}$ in calculating *CR* is minimal as confirmed by the high determination coefficient (R^2) of equation 2 (Fig. 1b), so that amphibole compositions with high F and oxo contents can be treated with this method with a sufficient accuracy.

In contrast, amphiboles with high Cl contents (e.g., Léger et al. 1996; Coogan et al. 2001) deviate significantly from equation 2 (towards lower *cmpg*) because the A_r value of chlorine is about twice that of F, OH and O. However, the maximum Cl content (i.e., 0.20 apfu, corresponding to 0.72 wt%) in the high-quality dataset produces negligible deviations from equation 2. This is because the incorporation of Cl in amphibole is always related to high Fe^{2+} contents (e.g., Oberti et al. 2007a) which results in relatively low *cmpg* underestimations (e.g., in the two Fe- and Cl-rich amphiboles marked with green triangles in Fig. 1b).

It is worth noting that equation 2 cannot be successfully applied to the original compositions of most of the amphiboles because EMP uncertainties commonly result in incorrect *CR* and *cmpg* values leading to significant deviations from the normalized composition, i.e., from total elements and oxides equal to 100 wt% (Fig. 1b). Therefore, at least a preliminary estimation of $^{W}O^{2-}$, H_2O and *TEO*, followed by a normalization calculation of the original composition, is required.

The oxo component, $^{W}O^{2-}$

It is commonly accepted that $^{W}O^{2-}$ and $^{W}OH^-$ contents in amphibole mostly depend on two substitution mechanisms involving cations occurring at the *M*(1) and *M*(3) sites (e.g., King et al. 1999; Popp et al. 2006; Oberti et al. 2007a):

$^{M(1)}(Mg, Fe^{2+}) + 2^{W}OH^{-} \rightarrow {}^{M(1)}Ti^{4+} + 2^{W}O^{2-}$ (a)

$^{M(1,3)}Fe^{2+} + {}^{W}OH^{-} \rightarrow {}^{M(1,3)}Fe^{3+} + {}^{W}O^{2-}$ (b)

During igneous and metamorphic processes, the OH^- content of amphibole is mostly ruled by substitution mechanism (a) wherein the amount of OH^- at the W site is reduced by twice the amount of Ti incorporated at the *M*(1) site. Substitution (a) mostly occurs at high-T low-fH_2O conditions, and involves chemical exchange of major components such as Mg, Fe^{2+} and Ti with the surrounding environment (i.e., minerals and melt). During magma ascent or hydrothermal alteration, amphibole may undergo a high T-fO_2 process of deprotonation (i.e., dehydrogenation) involving iron oxidation according to substitution mechanism (b).

From a crystal-chemical viewpoint, the occurrence of $^{W}O^{2-}$ induces important changes in the cation-ordering scheme typical of amphiboles, where high-charged C cations are fully ordered at the *M*(2) site, with the only exception of Al, which may disorder between the *M*(2) and *M*(3) sites in high-T Mg-rich pargasites and edenites (Oberti et al. 1995; Della Ventura et al. 2014). The different bond-valence bond-strength requirements of the O(3) oxygen after H^+ loss must be satisfied by the presence of high-charged cations at the coordinated *M*(1) (with multiplicity 2) and *M*(3) sites. This feature of the amphibole solid-solution system implies complex but strongly related compositional changes that can be empirically discerned using multivariate least-square analysis (e.g., Ridolfi and Renzulli 2012; Ridolfi et al. 2014; Zhang et al. 2017).

Among the 114 amphiboles in the calibration dataset, 87 formulae have $^{W}O^{2-} \leq 2^{C}Ti$ implying that mechanism (b) is almost not or weakly active. Hereafter, for these amphiboles we will use the prefix "poorly-oxidized" to remind that the amount of $^{M(1,3)}Fe^{3+}$ due to post-crystallization oxidation is zero or very low. These amphiboles may contain up to 1.3 apfu $^{W}O^{2-}$, which mostly derives from mechanism (a). However, the constraint of all the Ti in C-group cations (^{C}Ti) as a proxy for the oxo component (Hawthorne et al. 2012; Locock 2014) may be severely misleading because in these

samples a significant amount of ^{C}Ti is often ordered at the *M*(2) site and hence does not contribute to mechanism (a) (Oberti et al. 2007a).

Regression analysis shows that the $^{W}O^{2-}$ content in poorly-oxidized amphiboles (with $^{W}O^{2-} \leq 2^{C}Ti$) can be estimated with reasonably low errors (Fig. 2a) using the following equation:

$$^{W}O^{2-} = -6.684X_{Si} + 11.025X_{Ti} - 0.989X_{Al} - 2.800X_{Fetot} - 20.359X_{Mn} - 0.903X_{Mg} - 6.875X_{Ca} - 11.119X_{Na} - 2.553X_{K} + 5.751X_{F} + 4.610 \text{ apfu} \quad (3)$$

This equation can be applied without any previous calculation of the amphibole formula, as it only depends on the values of the cation fractions (X_i) calculated from EMP analyses. In addition, the X_i values are the same in both original and normalized compositions because a generalized overestimation (or underestimation) does not change the mass ratios.

A drawback of equation 3 is that it underestimates $^{W}O^{2-}$ in highly-oxidized amphiboles (where $^{W}O^{2-} > 2^{C}Ti$), which underwent high-T, high-fO_2 post-magmatic and/or hydrothermal alteration according to the mechanism (b). However, this issue may even turn out to be an advantage when studying the processes of magmatic crystallization from amphibole crystals which underwent post-magmatic oxidation-deprotonation. fO_2 in high-T magmatic environments (up to ~10^{-7} bar, corresponding to a logfO_2 of 3-4 units above the Ni-NiO buffer, hereafter NNO; Ridolfi and Renzulli 2012) is several orders of magnitude lower than in air (~0.21 bar, i.e., -0.68 logfO_2; Namur et al. 2012) where high-T post-magmatic oxidation most probably occurs. It is worth noting that the highly-oxidized amphiboles in our calibration dataset are Ca-dominant megacrysts (rapidly ejected to the surface from high T-P conditions) or mantle amphiboles crystallized from hydrothermal fluids (e.g. late-stage veins in peridotites, metasomatic deposits).

At this point, we analyzed correlations between the measured values of $^{W}O^{2-}$ and cation compositional parameters in both poorly and highly oxidized amphiboles, starting from the assumption that the fractions of Ti and Fe^{3+} occurring at the *M*(1) and *M*(3) sites are directly involved in the

process of deprotonation. The best correlation we found for the 114 amphiboles in the dataset is reported in Figure 2b: i.e., $^{W}O^{2-} = 0.963[4/3^{C}Ti + 2/3^{C}Fe^{3+} + 2/3^{A}(Na+K)] - 0.624$. The overall correlation shows a reasonably good R^2 value (0.927) and closely approaches the equation:

$$^{W}O^{2-} = 4/3^{C}Ti + 2/3^{C}Fe^{3+} + 2/3^{A}(Na+K) - 2/3 \text{ apfu} \quad (4a)$$

Equation 4a works well both for poorly ($^{W}O^{2-} \leq 2^{C}Ti$) and highly ($^{W}O^{2-} > 2^{C}Ti$) oxidized amphiboles when $4/3^{C}Ti + 2/3^{C}Fe^{3+} + 2/3^{A}(Na+K)$ is $\geq 2/3$. At those values, the only two samples significantly deviating from equation 4a (giving a $^{W}O^{2-}$ overestimation up to 0.49 apfu) are rare Na-Ca amphiboles, i.e., alumino-taramite K22-2 and fluoro-alumino-magnesio-taramite DJ102-23, which are characterized by high $^{C}Fe^{3+}$ and A-cation contents but, according to their crystal-chemical characterization do not contain oxo component (Oberti et al. 2007b; Fig. 2b). In Figure 2b, amphiboles with $4/3^{C}Ti + 2/3^{C}Fe^{3+} + 2/3^{A}(Na+K) \leq 2/3$ have zero or negligible $^{W}O^{2-}$ contents, providing the constraint:

$$^{W}O^{2-} = 0 \text{ apfu, if } 4/3^{C}Ti + 2/3^{C}Fe^{3+} + 2/3^{A}(Na+K) \leq 2/3 \text{ apfu} \quad (4b)$$

When applying equations 4a and constraint 4b we obtain a $\sigma_{est} = 0.12$ apfu for the whole dataset (Fig. 2b). When the two major outliers alumino-taramite K22-2 and fluoro-alumino-magnesio-taramite DJ102-23 are not considered, the maximum error decreases from 0.49 to 0.3 apfu which is even lower than that indicated by equation 3 for only the poorly-oxidized amphiboles (0.4 apfu; Fig. 2a).

Equation (4a) and constraint (4b) can be easily applied to any amphibole unit-formula anytime an independent measurement of Fe^{3+}/Fe_{tot} is available. When this is not the case, $^{W}O^{2-}$ and Fe^{3+} contents can be estimated using a system of two linear equations including (4a) and the charge balance equation:

$$4(Si+Ti) + 3(Al+Cr+Fe^{3+}) + 2[Mg+(Fe_{tot}-Fe^{3+})+Mn+Ni+Zn+Ca] + Na+K = 46 + {}^{W}O^{2-} \quad (4c)$$

where the uncertainty of the $^{W}O^{2-}$ and Fe^{3+} estimates depends on the errors of cation estimation multiplied by their ionic charge.

345 The presence of A-cations in equations (4a,b) may be explained by their capability to help in
346 achieving local electroneutrality around the O(3) site, where deprotonation occurs. Recent *in operando*
347 studies combining SREF and FTIR (Fourier Transform Infrared Spectroscopy) showed that
348 deprotonation preferentially occurs close to an occupied *A* site, so that it is faster in amphibole
349 compositions with fully occupied A-sites (Susta et al. 2016; Della Ventura et al. 2017; Oberti et al.
350 2018).
351

352 ## TOTAL COEFFICIENT AND CALCULATION PROCEDURE

353 In the previous section, we have stressed that the application of equation 2 is biased by the inevitable
354 EMP errors of the 114 high-quality amphibole data (Fig. 1). In order to overcome this problem,
355 obtaining an adjusted composition approaching a normalized one, we first calculated deviated
356 compositions which are the concentrations (wt%) of the oxides and halogens (F, Cl) calculated from a
357 normalized amphibole composition to have a *TEO* deviating from 100 wt% by a specific value, namely
358 98.2 and 101.8 wt%; e.g., normalized $SiO_2 \cdot 0.982$ (wt%), normalized $F \cdot 1.018$ (wt%). The opposites of
359 0.982 and 1.018 represent the corresponding total coefficients (*TC*) which, in general, can be calculated
360 by dividing the sum of the oxides of a normalized composition by that of its original or deviated
361 compositions. The *TC* values are 1 for normalized compositions, < 1 for overestimated compositions
362 and > 1 for underestimated compositions.

363 Then we used equations 2 and 3 to calculate preliminary formulas for both normalized and deviated
364 compositions. The values of Fe_2O_3 and FeO concentrations, $O^{F,Cl}$, and *Δcharge* can also be calculated
365 from these preliminary unit-formulae (Appendix 1). Multivariate least-square analysis using all of these
366 342 (114 normalized and 114·2 deviated) data provided the following equation to be used to calculate
367 *TC*:

$$TC = -7.9 * 10^{-4} SiO_2 + 6 * 10^{-4} TiO_2 - 6.6 * 10^{-4} Al_2O_3 + 8.75 * 10^{-5} Fe_2O_3 - 9.4 * 10^{-4} FeO - 8.5 * 10^{-4} MgO - 1.1 * 10^{-3} CaO - 1.48 * 10^{-3} Na_2O - 8.6 * 10^{-4} K_2O - 9.62 * 10^{-3} O^{F,Cl} + 6.41 * 10^{-3} H_2O - 9.57 * 10^{-3} TEO + 4.13 * 10^{-4} \Delta charge + 2.024 \quad (5)$$

where SiO_2 to K_2O are the original, normalized or the deviated oxides (wt%). The calculated regression parameters are $R^2 = 0.992$ and $\sigma_{est} = 0.001$ (Fig. 3).

If the *TC* values are applied to the original EMP analyses (i.e., original $SiO_2 \cdot TC$, original $TiO_2 \cdot TC$, etc.), the resulting adjusted compositions closely approach the normalized concentrations (wt%). These adjusted compositions can then be used to obtain amphibole formulae using again equations (2) and (3). Using the 114 amphiboles in our high-quality dataset, this second stage of calculations produces a statistic error (σ_{est}) of 0.055 apfu for ∑Si→K. The resulting formulae should be refined further using the series of stoichiometric constraints reported in Table 1 (see Appendix 1 for calculation).

When applying these constraints to the apfu calculated from the calibration dataset, only sporadic and very minor adjustments are observed (a few calculated formulae indicate ∑Si-K slightly higher than 16 apfu). In this dataset, the calculated *TEO* span from 99.6 to 100.5 wt%, and the final σ_{est} values for ^{A}(Ca+Na+K) and Si contents are 0.042 and 0.017 apfu, respectively (Table 3). The amount of Fe^{3+} (and Fe^{2+}) can then be calculated by charge balance (eq. 4c).

Optionally, the $^{W}O^{2-}$ and Fe^{3+} contents can be independently estimated using a system of two linear equations,i.e., 4a and 4c. The total amount of Fe^{2+} is finally calculated by the constraint $Fe_{tot} = Fe^{3+} + Fe^{2+}$ (Table 1, Appendix 1). The condition expressed in the constraint 4b should be respected and the priority in adjusting $^{W}O^{2-}$ and Fe^{3+} values should be given to charge balance (i.e., eq. 4c) considering that *Δcharge* can be as high as 0.1 due to error propagation in the solutions of this system.

Finally, the calculated amphibole formula (AMFORM) can be used to calculate the molecular mass (M_r), hereafter M_r^{AMFORM} (see section Essential Definitions for M_r calculation from a generic formula).

391 M_r^{AMFORM} should closely approach the molecular mass calculated with equation 1 using the *CR* value
392 obtained after the application of equation 1 to the adjusted compositions (hereafter $M_r^{CR} = 10^3 \cdot CR$
393 g/mol). In our database, the deviation among these molecular masses ($\Delta MM\% = 200\frac{M_r^{AMFORM} - M_r^{CR}}{M_r^{AMFORM} + M_r^{CR}}$)
394 ranges between -0.60 and 0.74% (σ_{est} = 0.18; Table 3).

395 A flowchart and a step by step procedure to calculate amphibole unit-formulae are reported in
396 Appendix 1. The whole procedure is included in a user-friendly Excel spreadsheet (provided as
397 supplementary material) called AMFORM.xlsx. By default, this spreadsheet gives the $^{W}O^{2-}$ and Fe^{3+}
398 values calculated according to equations 3 and 4c, but it also gives the results of the optional method
399 (eqs. 4a-c). We strongly recommend the use of this spreadsheet to avoid errors due to typing or
400 unavoidable approximations of the coefficients reported in this article.

401 AMFORM.xlsx also provides warnings for bad analyses and deviations from the correct
402 stoichiometry such as recalculated initial *TEO* < 98.2 and > 101.8 wt%, sum of C and B cations < 5 and
403 2 apfu, respectively (i.e., negative ΔC and Ca in A-group) and $\Delta MM\%$ < -0.60 and > 0.74%, which are
404 not included in Appendix 1.
405

406 ## TESTING THE AMFORM APPROACH

407 To allow for an independent validation of the AMFORM approach, a test was made using an additional
408 51 amphibole compositions belonging to the Ca, Na-Ca, Na and oxo groups, taken from the literature
409 (King et al. 2000; Tiepolo et al. 2001; Oberti et al. 2000, 2003, 2010, 2015, 2016, 2017; Uvarova et al.
410 2007; Satoh et al. 2004; Della Ventura et al. 2014; Gentili et al. 2015; Gatta et al. 2017) or still
411 unpublished (CNR-IGG Pavia), which have been analyzed with EMP±SREF±SIMS and other
412 techniques for Fe^{3+}/Fe_{tot} measurements ($KMnO_4$ titration, SXRF, XANES, Mössbauer spectroscopy). It
413 is worth noting that the analyses of these amphiboles generally have higher uncertainties (e.g., *TEO* of

97-102 wt%; *dC* from -0.07 to 0.01 apfu; *Δcharge* from -0.09 to 0.07) than the 114 analyses selected for the calibration of the AMFORM procedure (see the AMFORM spreadsheet for these lower-quality data). This second test dataset also includes 10 amphibole composition-formula pairs recently published by Dyar et al. (2016) respecting the quality criteria of the calibration data (AMFORM.xlsx).

Table 3 and Figure 4 compare the capability of AMFORM to estimate the amphibole formula parameters for both the calibration and the test data. The generally higher σ_{est} values of the lower-quality test data confirm the validity of our approach while the higher *ΔMM%* values indicate that this parameter is useful for detecting large analytical uncertainties (Table 3). The reliability of AMFORM is further confirmed by the homogeneous distribution around the 1:1 line observed for both calibration and test data and by the absence of outliers (Fig. 4). The few Li-free Na amphibole used to test AMFORM suggest that the method is reliable also in the case of Na amphiboles (e.g., Fig. 4c), for which the calibration was based solely on end-member compositions (Table 2; Fig. 1b). A test performed using 28 Fe-Mg-Mn *C*2/*m* species (cummingtonite-grunerite; Hirschmann et al. 1994) also suggest that AMFORM.xlsx can be used for these amphiboles with reasonably low uncertainties ($\sigma_{est} \leq$ 0.040 apfu for the main cations). However, this test is not reliable because Hirschmann et al. (1994) calculated the formula under the constraint that $\sum Si \rightarrow K = 15$.

A comparison between the AMFORM and the Locock (2014) spreadsheets

As a final step, we tested the capability of the most used methods to calculate the amphibole unit-formula (i.e., Tindle and Webb 1994; Dale et al. 2005; Locock 2014) using our calibration and test datasets (electronic supplement 1). For most compositions, the PROBE-AMPH spreadsheet (Tindle and Webb 1994) and the model of Dale et al. (2005) (which is an improvement of that of Holland and Blundy 1994) give errors which are about twice those of Locock (2014) and will be not discussed further.

When calculating the amphibole unit-formula, the most difficult parameters to quantify are the ^{C}Al and Fe^{3+}contents and the amount of cations in A, i.e., ^{A}(Ca + Na + K) (e.g., Leake et al. 1997; Al´meev et al. 2002; Ridolfi et al. 2010). Figure 5, compares the AMFORM results obtained for these parameters with those calculated by the spreadsheet published by Locock (2014), which is based on the procedures suggested in the IMA 2012 classification scheme (Hawthorne et al. 2012). When the Fe^{3+}/Fe_{tot} ratio, and/or the H_2O and Li contents are unknown (i.e., when only EMP analyses are available), the Locock (2014) spreadsheet provides two automatic procedures, depending on the presence or absence of $^{W}O^{2-}$. The Fe^{3+} contents resulting from AMFORM are those of the default $^{W}O^{2-}$ method (eq. 3 and 4c). As a matter of fact, considering the unit-formulae of the high-quality amphibole compositions as reference data (i.e., those cation contents that for their high-quality better approach the effective unit formulae), the errors of the AMFORM procedure are, on average, 2 to 4 times lower that those obtained with the spreadsheet proposed by Locock (2014) (Fig. 5).

Locock (2014) tends to underestimate ^{C}Al and ^{A}(Ca + Na + K) in amphiboles with total cation contents close to 16 apfu, and to slightly overestimate the same parameters when the ∑Si-K is close to 15 apfu. As far as the Fe^{3+} content is concerned, Locock (2014) methods with and without $^{W}O^{2-}$ estimates, behaves similarly to the 13- and 15-cations methods by IMA-1997 (Leake et al. 1997) as they generally produce large overestimations and large underestimations, respectively (Fig. 5).

For an independent validation of the AMFORM approach and Locock (2014)´s methods, we tested a subset of 19 published compositions of poorly-oxidized amphiboles (yellow squares in Fig. 5c; AMFORM spreadsheet). These data were not included in our high-quality calibration dataset because they were recently published, have not been examined by SREF and/or or because they have high *Δcharge* values (up to ±0.13). However, the Fe^{3+} content (and Fe^{3+}/Fe_{tot}) of these amphiboles should be valuable as it was estimated by SREF and Mössbauer spectroscopic analyses (Dyar et al. 2016), Synchroton X-ray Fluorescence (SXRF; King et al. 2000), $KMnO_4$ titration (Satoh et al. 2004) or X-ray

Absorption Near Edge Structure (XANES) spectroscopy (Bonadiman et al. 2014). In the AMFORM (default method) and Locock (2014) diagrams (Figs. 5c,f,i), these 19 amphiboles with $^{W}O^{2-} < 2Ti$ have the same behavior as the poorly-oxidized calibration amphiboles. When the reference Fe^{3+} values of these amphiboles are compared to those obtained by AMFORM, they approach the 1:1 line and have deviations (from -0.14 to +0.27 apfu) well within the maximum-minimum Fe^{3+} error range of the AMFORM default procedure (Fig. 5c).

An evaluation of the two methods used by AMFORM to calculate $^{W}O^{2-}$ and Fe^{3+}

Figure 6 reports plots and statistics obtained by using the AMFORM default (eq. 3, 4c) and the optional (eq. 4a-c) methods to calculate the $^{W}O^{2-}$ and Fe^{3+} contents for 137 amphibole compositions (114 high-quality compositions used for calibration plus 23 among lower-quality compositions and recently published data, both poorly and highly oxidized) where Fe^{3+}/Fe_{tot} values were measured as discussed in the previous paragraph and in Figure 5c.

The default method in AMFORM is particularly useful to estimate the amount of $^{W}O^{2-}$ and Fe^{3+} in poorly-oxidized amphiboles, those in equilibrium with the melt and/or other minerals (e.g., at 800–1,130 C, 130–2,200 MPa and in between NNO-2.1 and NNO+3.6; Ridolfi and Renzulli 2012). Indeed, these amphiboles fall very close to (and are distributed homogeneously around) the 1:1 line in Figures 6a,b; their $^{W}O^{2-}$ and Fe^{3+} contents can be estimated with a reasonably low uncertainty (±0.1 apfu; Table 3; Figs. 2a and 4c). In contrast, in the case of highly-oxidized amphiboles, i.e., those which underwent hydrothermal and post-crystallization oxidation, the default method may provide significant underestimation (up to 1.1 apfu, σ_{est} = 0.45 apfu; Fig. 6a,b), and therefore cannot be used to study metasomatic and oxidation processes during magma ascent (Dyar et al. 1993; King et al. 1999; Popp et al. 2006; Oberti et al. 2007a). Hence, we suggest to use the optional method for these amphiboles, because it provides a roughly homogeneous distribution around the 1:1 line in the plots in Figures 6d,e.

The large observed uncertainties when estimating $^{W}O^{2-}$ and Fe^{3+} values by this method (up to 1.1 apfu, σ_{est} = 0.3 apfu; Table 3) occur because of the substantial propagation of errors from the system of two linear equations (eq. 4a and 4c) and two variables ($^{W}O^{2-}$ and Fe^{3+}). Indeed, Table 3 also reports the estimated Fe^{3+} error due to uncertainty propagation (according to the probability theory), for both default and optional calculations. When calculated using the uncertainties of the calibration higher-quality dataset, the propagation of Fe^{3+} errors in the optional method are about twice of those in the default calculation and almost double when the quality of the data is lowered (i.e. when using the errors of the lower-quality test dataset). However, Figures 6c,f show that the error in Fe^{3+}/Fe_{tot} determination tends to decrease regularly with increasing total iron content (Fe_{tot}) for both the default (only considering the poorly-oxidized amphiboles) and the optional method. In other words, the tested amphiboles show a homogeneous and decreasing distribution around the zero-error line (Figs 6c,f). It is worth noting that the most used methods for unit-formula calculation (Tindle and Webb 1994; Dale et al. 2005; Locock 2014) result in much more scattered distributions of the Fe^{3+}/Fe_{tot} errors and higher σ_{est} values (electronic supplement 1). For Fe-Mg-Mn amphiboles such as cummingtonite and grunerite, we recommend the use of the optional method. We have tested AMFORM against the data of Hirschmann et al. (1994) indicating an $Fe^{3+}/Fe_{tot} \leq 1\%$ for heat-treated Fe-Mg-Mn amphiboles, as measured by Mössbauer spectroscopy (see above). For these amphiboles, the optional method shows $Fe^{3+}/Fe_{tot} < 5\%$ ($\leq 1\%$ for most of them, 71%) whereas the default method indicates higher Fe^{3+}/Fe_{tot} values (up to 17%).

IMPLICATIONS

Figure 4 and Table 3 demonstrate the capability of the AMFORM approach to quantify, based solely on EMP data, the most critical parameters in the unit formula of amphiboles with a satisfactory

509 reliability. It is worth noting that the proposed approach has been calibrated and is consistent with
510 crystal-chemical formulae obtained by combining high-quality structure refinement and analytical data.

511 The AMFORM procedure has been calibrated and validated for some petrologically-relevant
512 *C*2/*m* amphibole compositions (oxo, Ca, Na-Ca, Na, Fe-Mg-Mn amphiboles), considering only Li- and
513 Mn^{3+}-free end-member compositions. The presence of significant Li and Cl contents would strongly
514 affect the results because their lower cation mass and higher anion mass, respectively, would largely
515 affect the behavior of the *CR-cmpg* relationship. Indeed, AMFORM should be applied only to
516 amphiboles with Cl < 0.2 apfu (<1 wt%). In addition, AMFORM only accounts for Mn^{2+} and hence
517 cannot be used to constrain the formula of Mn^{3+}-rich amphiboles (e.g., dellaventuraite, ungarettiite;
518 Hawthorne et al. 1995; Hawthorne et al. 2012).

519 However, AMFORM.xlsx automatically provides warnings anytime the composition proposed
520 deviates too much from the calibration dataset and the calculated *TEO* values (both initial and adjusted)
521 deviate too much from those shown by the calibration amphiboles.

522 The default AMFORM procedure to estimate $^{W}O^{2-}$ and Fe^{3+} contents is particularly
523 recommended to study the stability of amphibole and develop (or refine) thermobarometric equations
524 aiming at constraining the magma pre-eruptive conditions and storage from the amphibole composition
525 of volcanic rocks (e.g., Ridolfi et al. 2010; Ridolfi and Renzulli 2012; Erdmann et al. 2014; Putirka
526 2016; Ridolfi et al. 2016). For this purpose, the difficulty of estimating the Fe^{3+} content related to
527 hydrothermal or post-magmatic oxidizing processes may even be considered as an advantage (see
528 above). In any case, this Fe^{3+} component can be roughly estimated using the optional $^{W}O^{2-}$ and Fe^{3+}
529 results in AMFORM.xlsx.

530 The mass-based method proposed in this work may also open a new perspective in the
531 calculation of the unit-formula of other minerals. It may be particularly useful for OH-bearing phases
532 characterized by structural vacancies, where the total number of cation is not known (e.g., micas).

While equation 1 is valid for any type of chemical compound and mineral, equation 2 must be adapted to other phases with different proportions of anion and cation sites in order to allow a reliable estimate of *CR*, and thus, of the total cation apfu contents.

Acknowledgments

This work was supported by a fellowship of the Alexander Von Humboldt Foundation and a research grant ("assegno di ricerca") co-funded by University of Perugia and University of Urbino through the Consolidator Grant ERC-2013- CoG Proposal No. 612776 CHRONOS (P.I. Diego Perugini), both awarded to the first author. AZ and RO acknowledge support by the Italian PRIN 2015 grant code 20158 A9CBM. We are grateful to R.R. Al´meev and O. Namur (Leibniz Universität Hannover) for their critical readings of the manuscript.

Careful and helpful reviews of the manuscript done by two anonymous referees greatly improved the quality of the manuscript. We thank them very much for all their suggestions.

References

Adam J., Oberti R., Cámara F., and Green T.H. (2007) An electron microprobe, LAM-ICP-MS and single-crystal X-ray structure refinement study of the effect of pressure, melt-H_2O concentration and fO_2 on experimentally produced basaltic amphiboles. European Journal of Mineralogy, 19, 641–655.

Al´meev R.R., Ariskin A.A., Ozerov A.Yu., and Kononkova N.N. (2002) Problems of the Stoichiometry and Thermobarometry of Magmatic Amphiboles: An Example of Hornblende

554 from the Andesites of Nezymyannyi Volcano, Eastern Kamchatka. Geochemistry International,
555 40, 723-738.

556 Bonadiman C., Nazzareni S., Coltorti M., Comodi P., Giuli G., and Faccini B. (2014) Crystal chemistry
557 of amphiboles: implications for oxygen fugacity and water activity in lithospheric mantle
558 beneath Victoria Land, Antarctica. Contributions to Mineralogy and Petrology, 167, 984.

559 Bottazzi P., Tiepolo M., Vannucci R., Zanetti A., Brumm R., Foley S.F., and Oberti R. (1999) Distinct
560 site preferences for heavy and light REE in amphibole and the prediction of $^{Amph/L}D_{REE}$.
561 Contributions to Mineralogy and Petrology, 137, 36-45.

562 Cipriani C. (2007) Amphiboles: Historical Perspective. Reviews in Mineralogy and Geochemitry, 67,
563 517-546.

564 Coogan L.A., Wilson R.N., Gillis K.M., and MacLeod C.J. (2001) Near-solidus evolution of oceanic
565 gabbros: insights from amphibole geochemistry. Geochimica et Cosmochimica Acta, 65, 4339–
566 4357.

567 Dale J., Powel R., White R.W., Elmer F.L., and Holland T.J.B. (2005) A thermodynamic model for
568 Ca–Na clinoamphiboles in Na_2O–CaO–FeO–MgO–Al_2O_3–SiO_2–H_2O–O for petrological
569 calculations. Journal of Metamorphic Geology, 23, 771–791.

570 Della Ventura G., Bellatreccia F., Cámara F., and Oberti R. (2014) Crystal-chemistry and short-range
571 order of fluoro-edenite and fluoro-pargasite: a combined X-ray diffraction and FTIR
572 spectroscopic approach. Mineralogical Magazine, 78, 293-310.

573 Della Ventura G., Susta U., Bellatreccia F., Marcelli A., Redhammer G.J., and Oberti R. (2017)
574 Deprotonation of Fe-dominant amphiboles: Single-crystal HT-FTIR spectroscopic studies of
575 synthetic potassic-ferro-richterite. American Mineralogist, 102, 117-125.

576 Dyar M.D., Mackwell S.J., McGuire A.V., Cross L.R., and Robertson J.D. (1993) Crystal chemistry of
577 Fe^{3+} and H^{+} in mantle kaersutite: Implications for mantle metasomatism. American Mineralogist,
578 78, 968-979.

579 Dyar M.D., Breves E.A., Gunter M.E., Lanzirotti A., Tucker J.M., Carey C.J., Peel S.E., Brown E.B.,
580 Oberti R., Lerotic M., and Delaney J.S. (2016) Use of multivariate analysis for synchrotron
581 micro-XANES analysis of iron valence state in amphiboles. American Mineralogist, 101, 1171–
582 1189.

583 Erdmann S., Martel C., Pichavant M., and Kushnir A. (2014) Amphibole as an archivist of magmatic
584 crystallization conditions: problems, potential, and implications for inferring magma storage
585 prior to the paroxysmal 2010 eruption of Mount Merapi, Indonesia. Contributions to Mineralogy
586 and Petrology, 167, 1016.

587 Esawi E.K. (2004) AMPH-CLASS: An Excel spreadsheet for the classification and nomenclature of
588 amphiboles based on the 1997 recommendations of the International Mineralogical Association.
589 Computers & Geosciences 30, 753–760.

590 Foley S., Tiepolo M., and Vannucci R. (2002) Growth of early continental crust controlled by melting
591 of amphibolite in subduction zones. Nature, 417, 837-840.

592 Forbes W.C., and Starmer R.J. (1974) Kaersutite is a possible source of alkali olivine basalts. Nature,
593 250, 209-210.

Gatta G.D., McIntyre G.J., Oberti R., and Hawthorne F.C. (2017) Order of $^{[6]}Ti^{4+}$ in a Ti-rich calcium amphibole from Kaersut, Greenland: a combined X-ray and neutron diffraction study. Physics and Chemistry of Minerals, 44, 83-94.

Gentili S., Bonadiman C., Biagioni C., Comodi P., Coltorti M., Zucchini A., and Ottolini L. (2015) Oxo-amphiboles in mantle xenoliths: evidence for H_2O-rich melt interacting with the lithospheric mantle of Harrow Peaks (Northern Victoria Land, Antarctica). Minerogy and Petrology, 109, 741-759.

Gunter M.E., Belluso E., and Mottana A. (2007) Amphiboles: Environmental and health concerns. Reviews in Mineralogy and Geochemitry, 67, 453-516.

Hammarstrom J.M., and Zen E. (1986) Aluminum in hornblende: an empirical igneous geobarometer. American Mineralogist, 71, 1297-1313.

Haüy R.J. (1822) Traité de Minéralogie. II ed. Bachelier-Huzard, Paris, pp. 597.

Hawthorne F.C., Ungaretti L., Oberti R., Bottazzi P., and Czamanske G.K. (1993) Li: An important component in igneous alkali amphiboles. American Mineralogist, 78, 733-745.

Hawthorne F.C. (1983) The crystal chemistry of the amphiboles. The Canadian Mineralogist, 21, 173-480 .

Hawthorne F.C., Oberti R., Cannillo E., Sardone N., Zanetti A., Grice J.D., and Ashley P.M. (1995). A new anhydrous amphibole from the Hoskins mine, Grenfell, New South Wales, Australia: Description and crystal structure of ungarettiite, $NaNa_2(Mn_2^{2+}Mn_3^{3+})Si_8O_{22}O_2$. American Mineralogist, 80, 165-172.

614 Hawthorne F.C., Oberti R., Della Ventura G., and Mottana A. (2007) Amphiboles: Crystal Chemistry,
615 Occurrence, and Health Issues. Reviews in Mineralogy and Geochemitry, 67, 545 pp

616 Hawthorne F.C., Oberti R., Harlow G.E., Maresch W.V., Martin R.F., Schumacher J.C., and Welch
617 M.D. (2012) IMA report Nomenclature of the amphibole supergroup. American Mineralogist,
618 97, 2031-2048.

619 Hawthorne F.C., Oberti R., Cannillo E., Ottolini L., Roelofsen J.N., and Martin R.F. (2001) Li-bearing
620 arfvedsonitic amphiboles from the Strange Lake peralkaline granite, Quebec. The Canadian
621 Mineralogist, 39, 1161-1170.

622 Hirschmann M., Evans B.W., and Yang H. (1994) Composition and temperature dependence of Fe-Mg
623 ordering in cummingtonite-grunerite as determined by X-ray diffraction. American Mineralogist
624 79, 862-877.

625 Holland T.J.B., and Blundy J.D. (1994) Non-ideal interactions in calcic amphiboles and their bearing
626 on amphibole-plagioclase thermometry. Contributions to Mineralogy and Petrology, 116, 433-
627 447.

628 Jackson C.R.M., Parman S.W., Kelley S.P., and Cooper R.F. (2013) Noble gas transport into the
629 mantle facilitated by high solubility in amphibole. Nature Geoscience, 6, 562-565.

630 Jacobson C.E., and Sorensen S.S. (1986) Amphibole compositions and metamorphic history of the
631 Rand Schist and the greenschist unit of the Catalina Schist, Southern California. Contributions to
632 Mineralogy and Petrology, 92, 308-315.

633 King P.L., Hervig R.L., Holloway J.R., Vennemann T.W., and Righter K. (1999) Oxy-substitution and
634 dehydrogenation in mantle-derived amphibole megacrysts. Geochimica et Cosmochimica Acta,
635 63, 3635-3651.

636 King P.L., Hervig R.L., Holloway J.R., Delaney J.S., and Dyar M.D. (2000) Partitioning of Fe^{3+}/Fe_{total}
637 between amphibole and basanitic melt as a function of oxygen fugacity. Earth and Planetary
638 Science Letters, 178, 97-112.

639 Laird J.O., and Albee A.L. (1981) High-pressure metamorphism in mafic schist from Northern
640 Vermont. American Journal of Science, 281, 97-126.

641 Léger A., Rebbert C., and Webster J. (1996) Cl-rich biotite and amphibole from Black Rock Forest,
642 Cornwall, New York. American Mineralogist, 81, 495–504.

643 Leake B.E. (1978) Nomenclature of amphiboles. The Canadian Mineralogist, 16, 501-520.

644 Leake B.E., Woolley A.R., Arps C.E.S., Birch W.D., Gilbert M.C., Grice J.D., Hawthorne F.C., Kato
645 A., Kisch H.J., Krivovichev V.G., Linthout K., Laird J., Mandarino J., Maresch W.V., Nickel
646 E.H., Schumaker J.C., Smith D.C., Stephenson N.C.N., Ungaretti L., Whittaker E.J.W., and
647 Youzhi G. (1997) Nomenclature of amphiboles: report of the subcommittee on amphiboles of
648 the International Mineralogical Association Commission on New Minerals and Mineral Names.
649 Mineralogical Magazine, 61, 295-321.

650 Locock A.J. (2014) An Excel spreadsheet to classify chemical analyses of amphiboles following the
651 IMA2012 recommendations. Computer and Geosciences, 62, 1–11.

652 McCanta M.C., Treiman A.H., Dyar M.D., Alexander C.M.O.'D., Rumble III D., and Essene E.J.
653 (2008) The LaPaz Icefield 04840 meteorite: Mineralogy, metamorphism, and origin of an
654 amphibole-and biotite-bearing R chondrite. Geochimica et Cosmochimica Acta, 72, 5757-5780.

655 Oberti R., Ungaretti L., Cannillo E., Hawthorne F.C., and Memmi I. (1995) Temperature-dependent Al
656 order-disorder in the tetrahedral double chain of C2/m amphiboles. European Journal of
657 Mineralogy, 7, 1049-1063.

658 Oberti R., Vannucci R., Zanetti A., Tiepolo M., and Brumm R.C. (2000) A crystal chemical re-
659 evaluation of amphibole/melt and amphibole/clinopyroxene D_{Ti} values in petrogenetic studies.
660 American Mineralogist, 85, 407-419.

661 Oberti R., Boiocchi M., and Smith D.C. (2003) Fluoronyböite from Jianchang (Su-Lu, China) and
662 nybo«ite from Nybö (Nordfjord, Norway): a petrological and crystal-chemical comparison of
663 these two high-pressure amphiboles. Mineralogical Magazine, 67, 769–782.

664 Oberti R., Hawthorne F.C., Cannillo E., and Cámara F. (2007a) Long-range order in amphiboles.
665 Reviews in Mineralogy and Geochemistry, 67, 125-171.

666 Oberti R., Boiocchi M., Smith D.C., and Medenbach O. (2007b) Aluminotaramite, alumino-
667 magnesiotaramite, and fuoro-alumino-magnesiotaramite: Mineral data and crystal chemistry.
668 American Mineralogist, 92, 1428-1435.

669 Oberti R., Boiocchi M., Hawthorne F.C., and Robinson P. (2010) Crystal structure and crystal
670 chemistry of fluoro-potassic-magnesio-arfvedsonite from Monte Metocha, Xixano region,
671 Mozambique, and discussion of the holotype from Quebec, Canada. Mineralogical Magazine,
672 74, 951-960.

673 Oberti R., Boiocchi M., Hawthorne F.C., Ball N.A., and Harlow G.E. (2015) Katophorite from the Jade
674 Mine Tract, Myanmar: mineral description of a rare (grandfathered) endmember of the
675 amphibole supergroup. Mineralogical Magazine, 79, 355–363.

676 Oberti R., Boiocchi M., Hawthorne F.C., Ball N.A., Cámara F., Pagano R., and Pagano A. (2016)
677 Ferro-ferri-hornblende from the Traversella Mine (Ivrea, Italy): occurrence, mineral description
678 and crystal-chemistry. Mineralogical Magazine, 80, 1233-1242.

679 Oberti R., Boiocchi M., Hawthorne F.C., Ball N.A., and Blass G. (2017) Ferri-obertiite from the
680 Rothenberg quarry, Eifel volcanic complex, Germany: mineral data and crystal chemistry of a
681 new amphibole end-member. Mineralogical Magazine, press. DOI: 10.1127/ejm/2018/0030-
682 2712.

683 Oberti R., Boiocchi M., Zema M., Hawthorne F.C., Redhammer G., Susta U., and Della Ventura G.
684 (2018) The HT behaviour of riebeckite: Expansivity, deprotonation, selective Fe oxidation and a
685 novel cation disordering scheme for amphiboles. European Journal of Mineralogy, press. DOI:
686 10.1127/ejm/2018/0030-2712.

687 Ottolini L., Bottazzi P., Zanetti A., and Vannucci R. (1995) Determination of hydrogen in silicates by
688 Second Ion Mass Spectrometry. The Analist, 120, 1309-1314.

689 Namur O., Charlier B., Toplis M.J., and Auwera J.V. (2012) Prediction of plagioclase-melt equilibria
690 in anhydrous silicate melts at 1 atm. Contributions to Mineralogy and Petrology, 163, 133-150.

691 Perinelli C., Andreozzi G.B., Conte A.M., Oberti R., and Armienti P. (2012) Redox state of
692 subcontinental lithospheric mantle and relationships with metasomatism: insights from spinel
693 peridotites from northern Victoria Land (Antarctica). Contributions to Mineralogy and
694 Petrology, 164, 1053-1067.

695 Popp R.K., Hibbert H.A., and Lamb W.M. (2006) Oxy-amphibole equilibria in Ti-bearing calcic
696 amphiboles: Experimental investigation and petrologic implications for mantle-derived
697 amphiboles. American Mineralogist, 91, 54-66.

698 Putirka K. (2016) Amphibole thermometers and barometers for igneous systems and some implications
699 for eruption mechanisms of felsic magmas at arc volcanoes. American Mineralogist, 101, 841–
700 858.

701 Ridolfi F., Renzulli A., and Puerini M. (2010) Stability and chemical equilibrium of amphibole in calc-
702 alkaline magmas: an overview, new thermobarometric formulations and application to
703 subduction-related volcanoes. Contributions to Mineralogy and Petrology, 160, 45-66.

704 Ridolfi F., and Renzulli A. (2012) Calcic amphiboles in calc-alkaline and alkaline magmas:
705 thermobarometric and chemometric empirical equations valid up to 1,130°C and 2.2 GPa.
706 Contributions to Mineralogy and Petrology, 163, 877-895.

707 Ridolfi F., Renzulli A., and Acosta-Vigil A. (2014) On the stability of magmatic cordierite and new
708 thermobarometric equations for cordierite-saturated liquids. Contributions to Mineralogy and
709 Petrology, 167, 996.

710 Ridolfi F., Braga R., Cesare B., Renzulli A., Perugini D., and Del Moro S. (2016) Unravelling the
711 complex interaction between mantle and crustal magmas encoded in the lavas of San Vincenzo
712 (Tuscany, Italy). Part I: Petrography and Thermobarometry. Lithos, 244, 218-232.

713 Robinson G.W., Grief J.D., Gault R.A., and Lalonde A.E. (1997) Potassic pargasite, a new member of
714 the amphibole group from Pargas, Turku-Pori, Finland. The Canadian Mineralogist, 35, 1535-
715 1540.

716 Rock N.M.S., and Leake B.E. (1984) The International Mineralogical Association amphibole
717 nomenclature scheme: computerization and its consequences. Mineralogical Magazine, 48, 211-
718 227.

719 Satoh H., Ymaguchi Y., and Makino K. (2004) Ti-substitution mechanism in plutonic oxy-kaersutite
720 from the Larvik alkaline complex, Oslo rift, Norway. Mineralogical Magazine, 68, 687–697.

721 Smith P.P.K. (1977) An Electron Microscopic Study of Amphibole Lamellae in Augite. Contributions
722 to Mineralogy and Petrology, 59, 317-322.

723 Smith D.J. (2014) Clinopyroxene precursors to amphibole sponge in arc crust. Nature
724 Communications, 5, 4329.

725 Spear F.S., and Kimball K.L. (1984). RECAMP—A FORTRAN IV program for estimating Fe^{3+}
726 contents in amphiboles. Computer and Geosciences, 10, 317-325.

727 Susta U. (2016) Dehydration and deprotonation processes in minerals: development of new
728 spectroscopic techniques. Unpublished PhD Thesis, University of Roma Tre.

729 Stout J.H. (1972) Phase Petrology and Mineral Chemistry of Coexisting Amphiboles from Telemark,
730 Norway. Journal of Petrology, 13, 99-145.

731 Tiepolo M., Vannucci R., Oberti R., Foley S., Bottazzi P., and Zanetti A. (2000) Nb and Ta
732 incorporation and fractionation in titanian pargasite and kaersutite: crystal-chemical constraints
733 and implications for natural systems. Earth and Planetary Science Letters, 176, 185-201.

734 Tiepolo M., Bottazzi P., Foley S.F., Oberti R., Vannucci R., and Zanetti A. (2001) Fractionation of Nb
735 and Ta from Zr and Hf at Mantle Depths: the Role of Titanian Pargasite and Kaersutite. Journal
736 of Petrology, 42, 221-232.

737 Tiepolo M., Zanetti A., Oberti R., Brumm R., Foley S., and Vannucci R. (2003) Trace-element
738 partitioning between synthetic potassic-richterites and silicate melts, and contrasts with the
739 partitioning behaviour of pargasites and kaersutites. European Journal of Mineralogy, 15, 329-
740 340.

741 Tindle A.G., and Webb P.C. (1994) PROBE-AMPH—a spreadsheet program to classify microprobe-
742 derived amphibole analyses. Computer and Geosciences, 20, 1201-1228.

743 Ungaretti L. (1980) Recent developments in X-ray single crystal diffractometry applied to the crystal-
744 chemical study of amphiboles. Godisnjak Jugoslavenskog Centra za Kristalografiju, 15, 29-65.

745 Ungaretti L., Smith D.C., and Rossi G. (1981) Crystal-chemistry by X-ray structure refinement and
746 electron microprobe analysis of a series of sodic-calcic to alkali amphiboles from the NybO
747 eclogite pod, Norway. Bulletin de Minéralogie, 104, 400-412.

748 Uvarova Y., Sokolova E., Hawthorne F.C., McCammon C.A., Kazansky V.I., and Lobanov K.V.
749 (2007) Amphiboles from the Kola Superdeep Borehole: Fe^{3+} contents from crystal-chemical
750 analysis and Mössbauer spectroscopy. Mineralogical Magazine, 71, 651-669.

751 Vannucci R., Piccardo G.B., Rivalenti G., Zanetti A., Rampone E., Ottolini L., Oberti R., Mazzucchelli
752 M., and Bottazzi P. (1995) Origin of LREE-depleted amphiboles in the subcontinental mantle.
753 Geochimica et Cosmochimica Acta, 59, 1763-1771.

754 Zhang J., Humphreys M.C.S., Cooper G.F., Davidson J.P., and Macpherson C.G. (2017) Magma mush
755 chemistry at subduction zones, revealed by new melt major element inversion from calcic
756 amphiboles. American Mineralogist, 102, 1353-1367.

Table captions

Table 1.

Summary of the preferred site-assignments and stoichiometric constraints for Li- and Mn^{3+}-free *C2/m* amphiboles, according to Hawthorne et al. (2012).

Table 2.

Formula and normalized composition (wt%) of the selected Li- and Mn-free monoclinic amphibole end-members and the oxo counterparts for the Ca amphiboles considered in this work. As the composition is normalized, all total elements and oxides close to ideality (100 wt%). The end-embers are ordered by increasing *Mr*. Values of *cmpg* are also reported for comparison.

Table 3.

Statistic errors (σ_{est}) of the AMFORM procedure calculated using the calibration and test data. The errors of uncertainty propagation in the calculation of the parameters are also reported. See AMFORM.xlsx for references and data.

Figure captions

Figure 1.

Plots of *CR* vs. (a) M_r, molecular mass, and (b) *cmpg*, cation mass per gram. The equations (and their statistic values) obtained using normalized and end-member (Table 2) compositions are also reported. The end-member sample with the lowest M_r is cummingtonite, $\square Mg_2Mg_5Si_8O_{22}(OH)_2$,

777 whereas that with the highest M_r is ferro-ferri-cannilloite, $CaCa_2(Fe^{2+}{}_4Fe^{3+})(Si_5Al_3)O_{22}(OH)_2$. Because
778 of EMP analytical errors, the original amphibole compositions show *TEO* (Total Elements and Oxides)
779 varying from 98.3 to 100.8 wt%. Underestimated (< 100 wt%) and overestimated (> 100 wt%)
780 compositions are located above and below the ideal relations, respectively. See the text for additional
781 details.
782
783 Figure 2.

784 (a) Correlation between the measured (reference) $^{W}O^{2-}$ values and those calculated with equation 3 for
785 87 amphiboles with $^{W}O^{2-} \leq 2^{C}Ti$ (i.e., poorly-oxidized amphiboles); the 1:1 line is reported together
786 with the standard (σ_{est}) and maximum (Max) errors. (b) The best correlation found between the
787 reference $^{W}O^{2-}$ values and cation composition for all the 114 high-quality amphibole compositions. The
788 red dashed lines describe the proposed relations; related equations and statistic errors are also reported
789 in red. See text for additional details.

790 Figure 3.

791 The correlation between *TC* (Total Coefficient) values and those calculated with equation 5 for the 342
792 calculated compositions (either normalized or deviated) and the 114 original compositions. Normalized
793 and deviated *TEO* data are also shown. Maximum and minimum uncertainties of the equation are
794 +0.005 and -0.004.

795 Figure 4.

796 The correlation between the reference ^{T}Si (a), ^{C}Al (b), ^{B}Na (c) and $^{A}(Ca + Na + K)$ (d) values and those
797 calculated with the AMFORM spreadsheet for the amphibole compositions used to calibrate the

798 procedure (blue diamonds) and for those used for testing (yellow triangles). The 1:1 lines are reported
799 in all diagrams (see Table 3 for statistics).

800 Figure 5.

801 Correlations between the reference ^{C}Al, ^{A}(Na + K + Ca) and Fe^{3+} values (from EMP+SREF±SIMS
802 data) and those calculated solely from the high-quality EMP analysis in our dataset; (a-c): AMFORM;
803 (d-f): Locock (2014) without $^{W}O^{2-}$ estimates; (g-i): Locock (2014) with $^{W}O^{2-}$ estimates. The statistics in
804 diagrams (c), (f), (i) for Fe^{3+} refer to the 87 amphiboles with $^{W}O^{2-} \leq 2^{C}$Ti, whereas all the other
805 diagrams refer to all the 114 amphiboles of the dataset; max and min errors are the maximum and
806 minimum (calculated – reference) values. Symbols are reported in (a) and (f). In (c), (f), (i), highly-
807 oxidized Ca amphiboles ($^{W}O^{2-} > 2^{C}$Ti) are distinguished by orange empty squares while yellow squares
808 are additional Ca and Na-Ca amphiboles (poorly-oxidized; $^{W}O^{2-} \leq 2^{C}$Ti) the Fe^{3+}/Fe_{tot} value of which
809 was measured using independent techniques (King et al. 2000; Satoh et al. 2004; Bonadiman et al.
810 2014; Dyar et al. 2016; see AMFORM.xlsx). The 1:1 line is reported in all diagrams.

811 Figure 6.

812 Correlations between the reference $^{W}O^{2-}$ and Fe^{3+} values and those calculated with the default (a-b) and
813 the optional (d-e) procedures in AMFORM for the 114 compositions used for calibration and the 23
814 compositions with Fe^{3+} measured by independent techniques. In these diagrams the 1:1 line is also
815 shown. (c) and (f) report the errors of Fe^{3+}/Fe_{tot} calculations versus the reference total iron content
816 (apfu); the line represent the 0 error reference. In (a) and (b), statistics refer only to highly-oxidized Ca
817 amphiboles (with $^{W}O^{2-} > {}^{C}$Ti) and ferri-kaersutites, symbols have the same color of statistic values; see
818 Fig. 4c for the statistics of poorly-oxidized amphiboles. In (c), (d), (e) and (f) statistics refer to all the
819 137 amphiboles considered. See the text for additional explanations.

Fig 1.

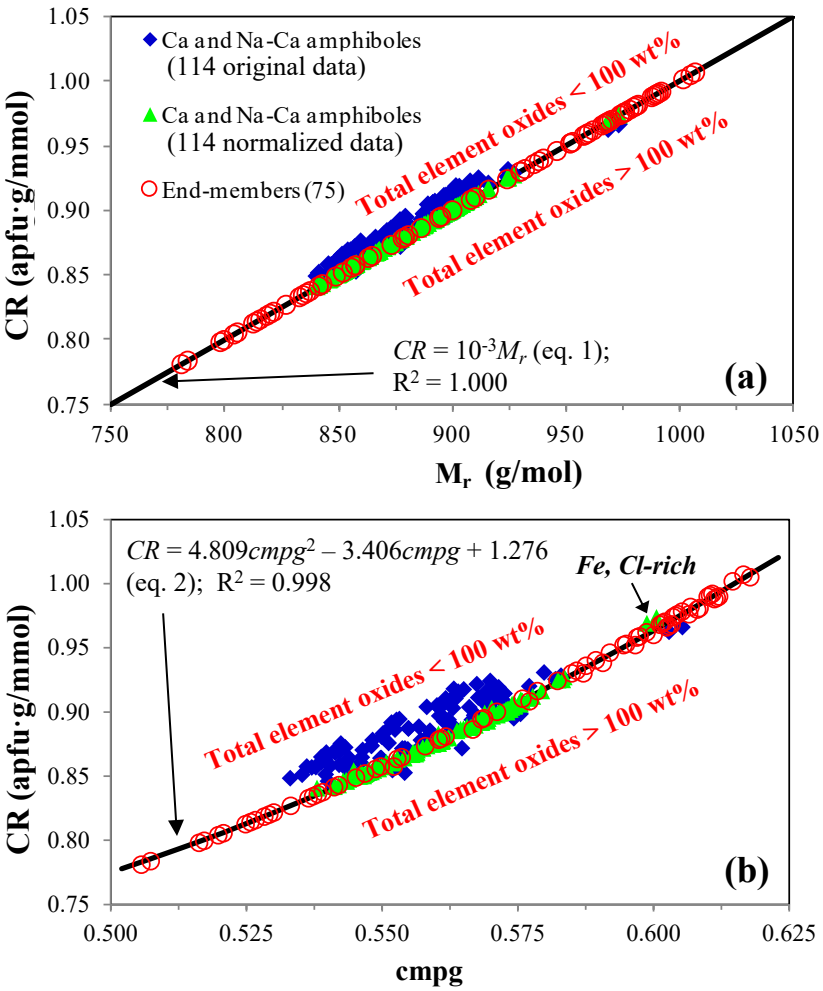
Ca and Na-Ca amphiboles (114 original data)
Ca and Na-Ca amphiboles (114 normalized data)
End-members (75)
Total element oxides < 100 wt%
Total element oxides > 100 wt%
CR = 10-3Mr (eq. 1); R2 = 1.000
(a)
CR (apfu·g/mmol)
Mr (g/mol)
CR = 4.809cmpg2 – 3.406cmpg + 1.276 (eq. 2); R2 = 0.998
Fe, Cl-rich
Total element oxides < 100 wt%
Total element oxides > 100 wt%
(b)
CR (apfu·g/mmol)
cmpg

Fig 2.

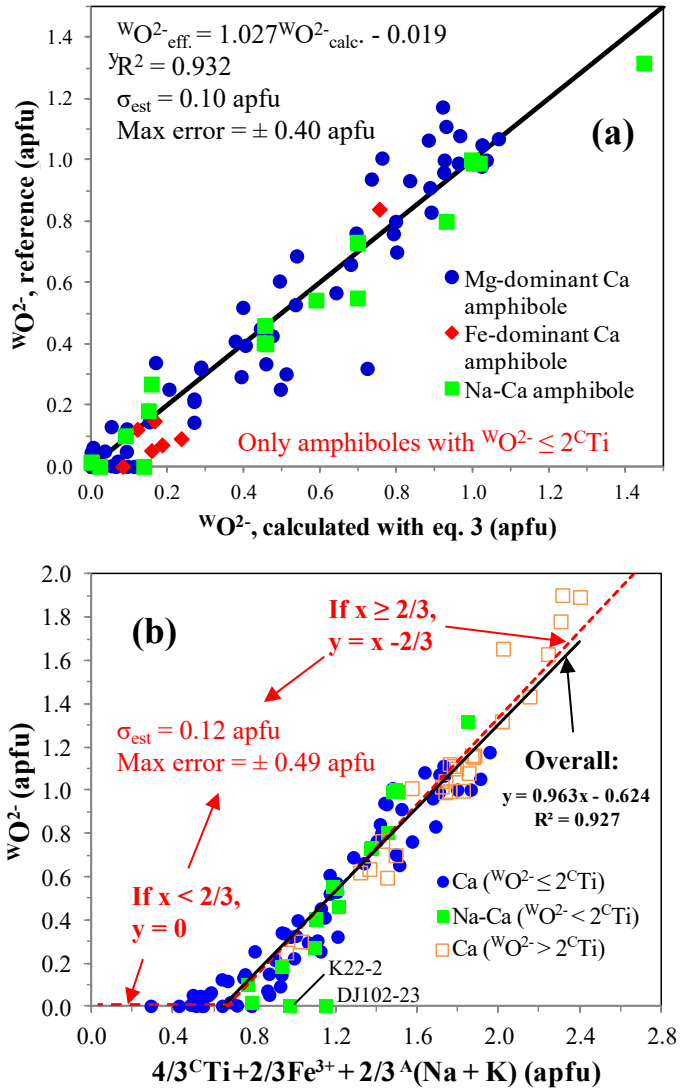
$^{W}O^{2-}_{eff.} = 1.027\,^{W}O^{2-}_{calc.} - 0.019$
$^{y}R^2 = 0.932$
σ_{est} = 0.10 apfu
Max error = ± 0.40 apfu
(a)
Mg-dominant Ca amphibole
Fe-dominant Ca amphibole
Na-Ca amphibole
Only amphiboles with $^{W}O^{2-} \leq 2^{C}Ti$
$^{W}O^{2-}$, reference (apfu)
$^{W}O^{2-}$, calculated with eq. 3 (apfu)
(b)
If x ≥ 2/3, y = x -2/3
σ_{est} = 0.12 apfu
Max error = ± 0.49 apfu
If x < 2/3, y = 0
Overall:
y = 0.963x - 0.624
R² = 0.927
Ca ($^{W}O^{2-} \leq 2^{C}Ti$)
Na-Ca ($^{W}O^{2-} < 2^{C}Ti$)
Ca ($^{W}O^{2-} > 2^{C}Ti$)
K22-2
DJ102-23
$^{W}O^{2-}$ (apfu)
$4/3^{C}Ti+2/3Fe^{3+}+2/3\,^{A}(Na+K)$ (apfu)

Fig 3.

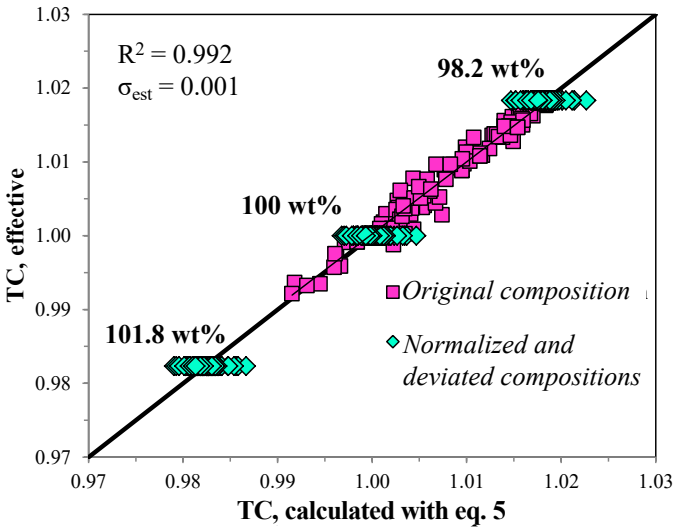
R2 = 0.992
σest = 0.001
98.2 wt%
100 wt%
101.8 wt%
Original composition
Normalized and deviated compositions
TC, effective
TC, calculated with eq. 5
1.03
1.02
1.01
1.00
0.99
0.98
0.97
0.97
0.98
0.99
1.00
1.01
1.02
1.03

Fig 4.

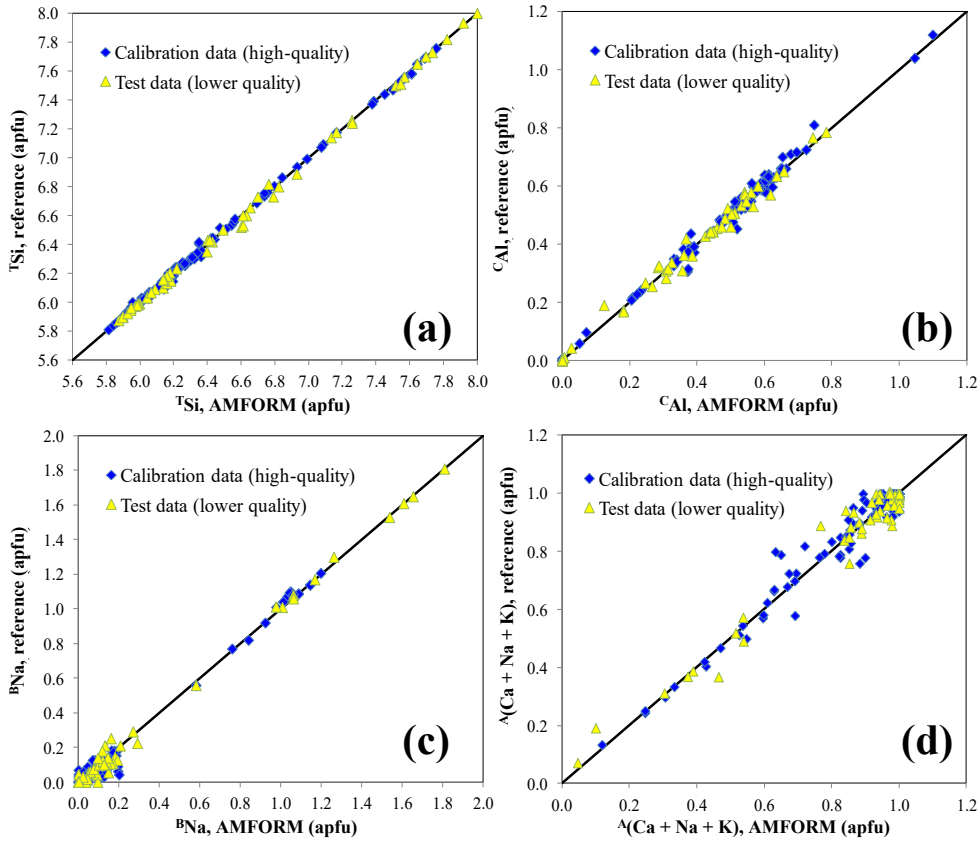
Calibration data (high-quality)
Test data (lower quality)
(a)
TSi, reference (apfu)
TSi, AMFORM (apfu)
(b)
CAl, reference (apfu)
CAl, AMFORM (apfu)
(c)
BNa, reference (apfu)
BNa, AMFORM (apfu)
(d)
A(Ca + Na + K), reference (apfu)
A(Ca + Na + K), AMFORM (apfu)

Fig 5.

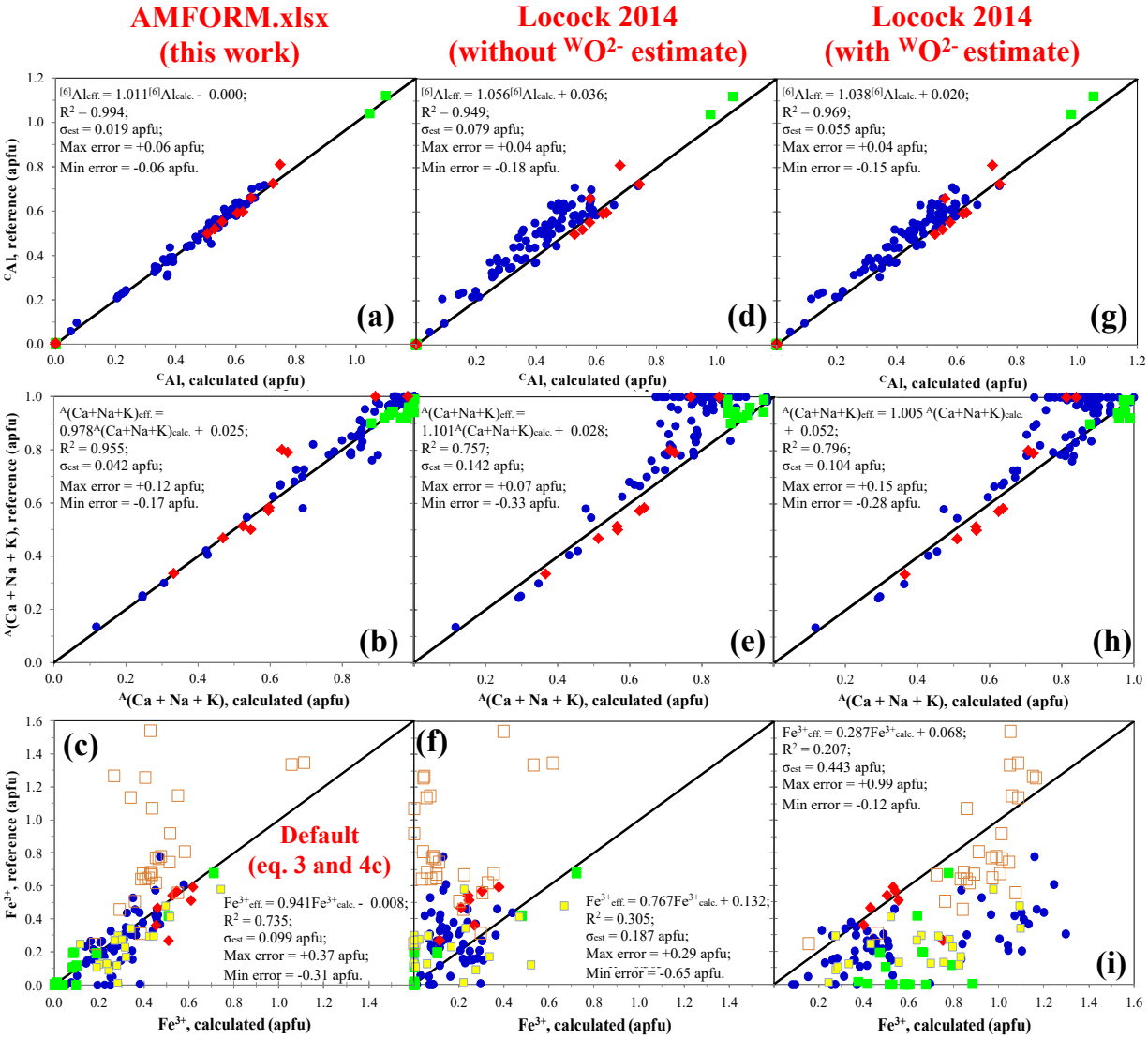
AMFORM.xlsx
(this work)
Locock 2014
(without WO2- estimate)
Locock 2014
(with WO2- estimate)
[6]Aleff. = 1.011[6]Alcalc. - 0.000;
R2 = 0.994;
σest = 0.019 apfu;
Max error = +0.06 apfu;
Min error = -0.06 apfu.
(a)
[6]Aleff. = 1.056[6]Alcalc. + 0.036;
R2 = 0.949;
σest = 0.079 apfu;
Max error = +0.04 apfu;
Min error = -0.18 apfu.
(d)
[6]Aleff. = 1.038[6]Alcalc. + 0.020;
R2 = 0.969;
σest = 0.055 apfu;
Max error = +0.04 apfu;
Min error = -0.15 apfu.
(g)
CAl, reference (apfu)
CAl, calculated (apfu)
A(Ca+Na+K)eff. =
0.978A(Ca+Na+K)calc. + 0.025;
R2 = 0.955;
σest = 0.042 apfu;
Max error = +0.12 apfu;
Min error = -0.17 apfu.
(b)
A(Ca+Na+K)eff. =
1.101A(Ca+Na+K)calc. + 0.028;
R2 = 0.757;
σest = 0.142 apfu;
Max error = +0.07 apfu;
Min error = -0.33 apfu.
(e)
A(Ca+Na+K)eff. = 1.005 A(Ca+Na+K)calc.
+ 0.052;
R2 = 0.796;
σest = 0.104 apfu;
Max error = +0.15 apfu;
Min error = -0.28 apfu.
(h)
A(Ca + Na + K), reference (apfu)
A(Ca + Na + K), calculated (apfu)
(c)
Default
(eq. 3 and 4c)
Fe3+eff. = 0.941Fe3+calc. - 0.008;
R2 = 0.735;
σest = 0.099 apfu;
Max error = +0.37 apfu;
Min error = -0.31 apfu.
(f)
Fe3+eff. = 0.767Fe3+calc. + 0.132;
R2 = 0.305;
σest = 0.187 apfu;
Max error = +0.29 apfu;
Min error = -0.65 apfu.
Fe3+eff. = 0.287Fe3+calc. + 0.068;
R2 = 0.207;
σest = 0.443 apfu;
Max error = +0.99 apfu;
Min error = -0.12 apfu.
(i)
Fe3+, reference (apfu)
Fe3+, calculated (apfu)

Fig 6.

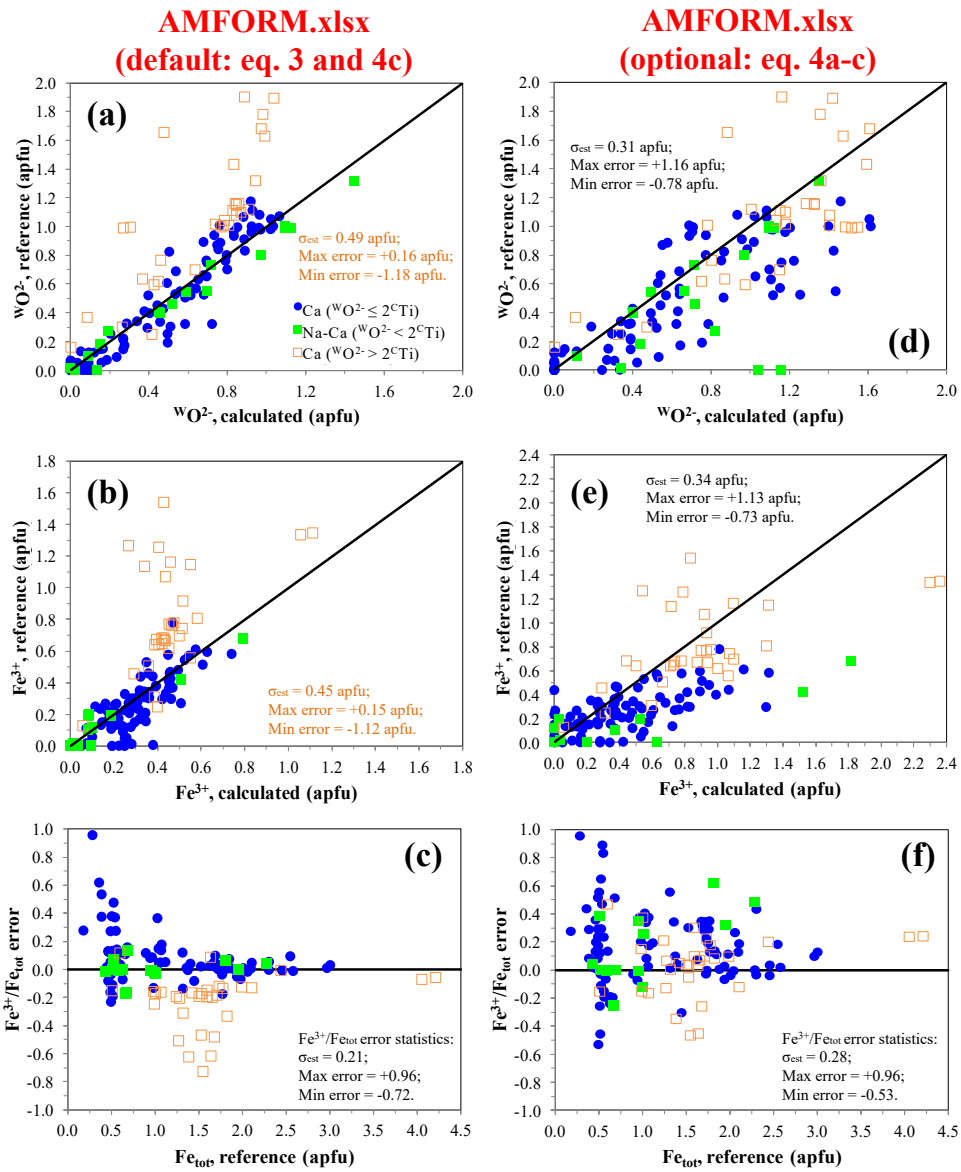
AMFORM.xlsx
(default: eq. 3 and 4c)
AMFORM.xlsx
(optional: eq. 4a-c)
(a)
(b)
(c)
(d)
(e)
(f)
σest = 0.49 apfu;
Max error = +0.16 apfu;
Min error = -1.18 apfu.
Ca (WO2- ≤ 2CTi)
Na-Ca (WO2- < 2CTi)
Ca (WO2- > 2CTi)
σest = 0.45 apfu;
Max error = +0.15 apfu;
Min error = -1.12 apfu.
Fe3+/Fetot error statistics:
σest = 0.21;
Max error = +0.96;
Min error = -0.72.
σest = 0.31 apfu;
Max error = +1.16 apfu;
Min error = -0.78 apfu.
σest = 0.34 apfu;
Max error = +1.13 apfu;
Min error = -0.73 apfu.
Fe3+/Fetot error statistics:
σest = 0.28;
Max error = +0.96;
Min error = -0.53.
WO2-, reference (apfu)
WO2-, calculated (apfu)
Fe3+, reference (apfu)
Fe3+, calculated (apfu)
Fe3+/Fetot error
Fetot, reference (apfu)

TABLE 1. Summary of the preferred site assignments and stoichiometric constraints for Li- and Mn^{3+}-free *C*2/*m* amphiboles, according to Hawthorne et al. (2012)

Site-groups and total occupancy		Elements	Stoichiometric constraints (apfu)
		Cations (15–16 apfu)	
T (8 apfu)	C (5 apfu)	Si	Si ≤ 8
		Al	
		Ti	∑Si→Ti ≥ 8
		Cr	
		Ni	
		Zn	
		Fe_{tot}	
		Mn	
B (2 apfu)		Mg	∑Si→Mg ≥ 13
	A (0–1 apfu)	Ca	
		Na	
		K	15 ≤ ∑Si→K ≤ 16
		Anions (24 apfu)	
O (22 apfu)	W (2 apfu)	O	∑O ≥ 22
		OH	
		F	
		Cl	

Notes: apfu = atoms per formula unit; ΔC = ΣSi→Mg – 13 (Mn, Fe^{2+}, and Mg occurring as B cations). $Fe_{tot} = Fe^{3+} + Fe^{2+}$ (only Fe^{2+} is assigned to the B sites).

Table 2

Name	Group	Sub-group	Formula	SiO_2	TiO_2	Al_2O_3	FeO_{tot}	MgO	CaO	Na_2O	Sum	Fe_2O_3	FeO	H_2O	M_r	*cmpg*
Cummingtonite	^{W}(OH,F,Cl)	Mg-Fe-Mn	$\square Mg_2Mg_5Si_8O_{22}(OH)_2$	61.56	0.00	0.00	0.00	36.13	0.00	0.00	97.69			2.31	781	0.506
Glaucophane	^{W}(OH,F,Cl)	Na	$\square Na_2(Mg_3Al_2)Si_8O_{22}(OH)_2$	61.35	0.00	13.01	0.00	15.43	0.00	7.91	97.70			2.30	784	0.507
Winchite	^{W}(OH,F,Cl)	Na-Ca	$\square(NaCa)(Mg_4Al)Si_8O_{22}(OH)_2$	60.24	0.00	6.39	0.00	20.20	7.03	3.88	97.74			2.26	798	0.516
Barroisite	^{W}(OH,F,Cl)	Na-Ca	$\square(NaCa)(Mg_3Al_2)(Si_7Al)O_{22}(OH)_2$	52.60	0.00	19.13	0.00	15.12	7.01	3.88	97.75			2.25	800	0.517
Eckermannite	^{W}(OH,F,Cl)	Na	$NaNa_2(Mg_4Al)Si_8O_{22}(OH)_2$	59.80	0.00	6.34	0.00	20.06	0.00	11.57	97.76			2.24	804	0.520
Nybøite	^{W}(OH,F,Cl)	Na	$NaNa_2(Mg_3Al_2)(Si_7Al)O_{22}(OH)_2$	52.22	0.00	18.99	0.00	15.01	0.00	11.54	97.76			2.24	805	0.521
Tremolite	^{W}(OH,F,Cl)	Ca	$\square Ca_2Mg_5Si_8O_{22}(OH)_2$	59.17	0.00	0.00	0.00	24.81	13.81	0.00	97.78			2.22	812	0.525
Magnesio-hornblende	^{W}(OH,F,Cl)	Ca	$\square Ca_2(Mg_4Al)(Si_7Al)O_{22}(OH)_2$	51.67	0.00	12.53	0.00	19.81	13.78	0.00	97.79			2.21	814	0.526
Tschermakite	^{W}(OH,F,Cl)	Ca	$\square Ca_2(Mg_3Al_2)(Si_6Al_2)O_{22}(OH)_2$	44.21	0.00	25.01	0.00	14.83	13.75	0.00	97.79			2.21	815	0.527
Richterite	^{W}(OH,F,Cl)	Na-Ca	$Na(NaCa)Mg_5Si_8O_{22}(OH)_2$	58.74	0.00	0.00	0.00	24.63	6.85	7.57	97.80			2.20	818	0.528
Katophorite	^{W}(OH,F,Cl)	Na-Ca	$Na(NaCa)(Mg_4Al)(Si_7Al)O_{22}(OH)_2$	51.30	0.00	12.44	0.00	19.66	6.84	7.56	97.80			2.20	820	0.529
Taramite	^{W}(OH,F,Cl)	Na-Ca	$Na(NaCa)(Mg_3Al_2)(Si_6Al_2)O_{22}(OH)_2$	43.89	0.00	24.83	0.00	14.72	6.83	7.55	97.81			2.19	821	0.530
Ferri-winchite	^{W}(OH,F,Cl)	Na-Ca	$\square(NaCa)(Mg_4Fe^{3+})Si_8O_{22}(OH)_2$	58.14	0.00	0.00	8.69	19.50	6.78	3.75	96.85	9.66	0.00	2.18	827	0.533
Magnesio-arfvedsonite	^{W}(OH,F,Cl)	Na	$NaNa_2(Mg_4Fe^{3+})Si_8O_{22}(OH)_2$	57.72	0.00	0.00	8.63	19.36	0.00	11.16	96.88	9.59	0.00	2.16	833	0.536
Edenite	^{W}(OH,F,Cl)	Ca	$NaCa_2Mg_5(Si_7Al)O_{22}(OH)_2$	50.41	0.00	6.11	0.00	24.16	13.44	3.71	97.84			2.16	834	0.537
Pargasite	^{W}(OH,F,Cl)	Ca	$NaCa_2(Mg_4Al)(Si_6Al_2)O_{22}(OH)_2$	43.13	0.00	18.30	0.00	19.29	13.42	3.71	97.84			2.16	836	0.538
Sadanagaite	^{W}(OH,F,Cl)	Ca	$NaCa_2(Mg_3Al_2)(Si_5Al_3)O_{22}(OH)_2$	35.88	0.00	30.44	0.00	14.44	13.39	3.70	97.85			2.15	837	0.539
Magnesio-riebeckite	^{W}(OH,F,Cl)	Na	$\square Na_2(Mg_3Fe^{3+}{}_2)Si_8O_{22}(OH)_2$	57.14	0.00	0.00	17.08	14.37	0.00	7.37	95.96	18.98	0.00	2.14	841	0.541
Magnesio-ferri-hornblende	^{W}(OH,F,Cl)	Ca	$\square Ca_2(Mg_4Fe^{3+})(Si_7Al)O_{22}(OH)_2$	49.90	0.00	6.05	8.52	19.13	13.31	0.00	96.91	9.47	0.00	2.14	843	0.542
Ferri-katophorite	^{W}(OH,F,Cl)	Na-Ca	$Na(NaCa)(Mg_4Fe^{3+})(Si_7Al)O_{22}(OH)_2$	49.56	0.00	6.01	8.47	19.00	6.61	7.30	96.93	9.41	0.00	2.12	849	0.545
Cannilloite	^{W}(OH,F,Cl)	Ca	$CaCa_2(Mg_4Al)(Si_5Al_3)O_{22}(OH)_2$	35.27	0.00	23.94	0.00	18.93	19.75	0.00	97.89			2.11	852	0.547
Rootname 4	^{W}(OH,F,Cl)	Ca	$NaCa_2(Mg_4Ti)(Si_5Al_3)O_{22}(OH)_2$	35.11	9.33	17.88	0.00	18.84	13.11	3.62	97.89			2.11	856	0.549
Kaersutite	^{W}O	-	$NaCa_2(Mg_3TiAl)(Si_6Al_2)O_{22}O_2$	42.05	9.32	17.84	0.00	14.10	13.08	3.61	100.00			0.00	857	0.552
Ferri-barroisite	^{W}(OH,F,Cl)	Na-Ca	$Na(NaCa)(Mg_3Fe^{3+}2)(Si_7Al)O_{22}(OH)_2$	49.06	0.00	5.95	16.76	14.10	6.54	3.61	96.03	18.63	0.00	2.10	857	0.550
Ferri-nybøite	^{W}(OH,F,Cl)	Na	$NaNa_2(Mg_3Fe^{3+}{}_2)(Si_7Al)O_{22}(OH)_2$	48.73	0.00	5.91	16.65	14.01	0.00	10.77	96.06	18.50	0.00	2.09	863	0.553
Magnesio-hastingsite	^{W}(OH,F,Cl)	Ca	$NaCa_2(Mg_4Fe^{3+})(Si_6Al_2)O_{22}(OH)_2$	41.69	0.00	11.79	8.31	18.64	12.97	3.58	96.99	9.23	0.00	2.08	865	0.554
Ferri-tschermakite	^{W}(OH,F,Cl)	Ca	$\square Ca_2(Mg_3Fe^{3+}{}_2)(Si_6Al_2)O_{22}(OH)_2$	41.28	0.00	11.68	16.45	13.85	12.84	0.00	96.10	18.29	0.00	2.06	873	0.558
Ferro-glaucophane	^{W}(OH,F,Cl)	Na	$\square Na_2(Fe^{2+}{}_3Al_2)Si_8O_{22}(OH)_2$	54.74	0.00	11.61	24.54	0.00	0.00	7.06	97.95	0.00	24.54	2.05	878	0.560
Ferri-taramite	^{W}(OH,F,Cl)	Na-Ca	$Na(NaCa)(Mg_3Fe3+_2)(Si_6Al_2)O_{22}(OH)_2$	41.01	0.00	11.60	16.34	13.75	6.38	7.05	96.13	18.16	0.00	2.05	879	0.561
Ferri-cannilloite	^{W}(OH,F,Cl)	Ca	$CaCa_2(Mg_4Fe^{3+})(Si_5Al_3)O_{22}(OH)_2$	34.11	0.00	17.37	8.16	18.31	19.10	0.00	97.05	9.07	0.00	2.05	881	0.562
Ferri-kaersutite	^{W}O	-	$NaCa_2(Mg_3TiFe^{3+})(Si_6Al_2)O_{22}O_2$	40.68	9.01	11.51	8.11	13.64	12.66	3.50	99.10	9.01	0.00	0.00	886	0.567
Ferro-barroisite	^{W}(OH,F,Cl)	Na-Ca	$\square(NaCa)(Fe^{2+}{}_3Al_2)(Si_7Al)O_{22}(OH)_2$	47.04	0.00	17.10	24.11	0.00	6.27	3.47	97.99	0.00	24.11	2.01	894	0.568
Ferri-sadanagaite	^{W}(OH,F,Cl)	Ca	$NaCa_2(Mg_3Fe^{3+}{}_2)(Si_5Al_3)O_{22}(OH)_2$	33.56	0.00	17.09	16.05	13.51	12.53	3.46	96.20	17.84	0.00	2.01	895	0.569
Ferro-nybøite	^{W}(OH,F,Cl)	Na	$NaNa_2(Fe^{2+}{}_3Al_2)(Si_7Al)O_{22}(OH)_2$	46.73	0.00	16.99	23.95	0.00	0.00	10.33	98.00	0.00	23.95	2.00	900	0.571
oxo Ferro-tschermakite	^{W}O	Ca	$\square Ca_2(Fe^{2+}Fe^{3+}{}_2Al_2)(Si_6Al_2)O_{22}O_2$	39.70	0.00	22.46	23.73	0.00	12.35	0.00	98.24	17.58	7.91	0.00	908	0.577
Ferro-tschermakite	^{W}(OH,F,Cl)	Ca	$\square Ca_2(Fe^{2+}{}_3Al_2)(Si_6Al_2)O_{22}(OH)_2$	39.61	0.00	22.41	23.68	0.00	12.32	0.00	98.02	0.00	23.68	1.98	910	0.576
Ferro-taramite	^{W}(OH,F,Cl)	Na-Ca	$Na(NaCa)(Fe^{2+}{}_3Al_2)(Si_6Al_2)O_{22}(OH)_2$	39.35	0.00	22.26	23.53	0.00	6.12	6.77	98.03	0.00	23.53	1.97	916	0.579
Ferro-winchite	^{W}(OH,F,Cl)	Na-Ca	$\square(NaCa)(Fe2+4Al)Si8O22(OH)2$	52.01	0.00	5.52	31.10	0.00	6.07	3.35	98.05	0.00	31.10	1.95	924	0.582
oxo Ferro-sadanagaite	^{W}O	Ca	$NaCa_2(Fe^{2+}Fe^{3+}{}_2Al_2)(Si_5Al_3)O_{22}O_2$	32.30	0.00	27.41	23.18	0.00	12.06	3.33	98.28	17.17	7.73	0.00	930	0.587
Ferro-eckermannite	^{W}(OH,F,Cl)	Na	$NaNa_2(Fe^{2+}{}_4Al)Si_8O_{22}(OH)_2$	51.68	0.00	5.48	30.90	0.00	0.00	10.00	98.06	0.00	30.90	1.94	930	0.585
Ferro-sadanagaite	^{W}(OH,F,Cl)	Ca	$NaCa_2(Fe^{2+}{}_3Al_2)(Si_5Al_3)O_{22}(OH)_2$	32.23	0.00	27.35	23.13	0.00	12.03	3.33	98.07	0.00	23.13	1.93	932	0.586
Riebeckite	^{W}(OH,F,Cl)	Na	$\square Na_2(Fe^{2+}{}_3Fe^{3+}{}_2)Si_8O_{22}(OH)_2$	51.36	0.00	0.00	38.38	0.00	0.00	6.62	96.37	17.06	23.03	1.92	936	0.588
oxo Ferro-hornblende	^{W}O	Ca	$\square Ca_2(Fe^{2+}{}_2Fe^{3+}{}_2Al)(Si_7Al)O_{22}O_2$	44.83	0.00	10.87	30.63	0.00	11.96	0.00	98.29	17.02	15.32	0.00	938	0.591
Ferro-hornblende	^{W}(OH,F,Cl)	Ca	$\square Ca_2(Fe^{2+}{}_4Al)(Si_7Al)O_{22}(OH)_2$	44.74	0.00	10.85	30.57	0.00	11.93	0.00	98.08	0.00	30.57	1.92	940	0.589
Ferro-katophorite	^{W}(OH,F,Cl)	Na-Ca	$Na(NaCa)(Fe^{2+}{}_4Al)(Si_7Al)O_{22}(OH)_2$	44.46	0.00	10.78	30.38	0.00	5.93	6.55	98.10	0.00	30.38	1.90	946	0.592
Ferro-ferri-barroisite	^{W}(OH,F,Cl)	Na-Ca	$\square(NaCa)(Fe^{2+}{}_3Fe^{3+}{}_2)(Si_7Al)O_{22}(OH)_2$	44.19	0.00	5.36	37.74	0.00	5.89	3.26	96.43	16.78	22.64	1.89	952	0.594
Ferro-kaersutite	^{W}O	-	$NaCa_2(Fe^{2+}{}_3TiAl)(Si_6Al_2)O_{22}O_2$	37.87	8.39	16.07	22.64	0.00	11.78	3.26	100.00	0.00	22.64	0.00	952	0.597
Ferro-ferri-winchite	^{W}(OH,F,Cl)	Na-Ca	$\square(NaCa)(Fe^{2+}{}_4Fe^{3+})Si_8O_{22}(OH)_2$	50.44	0.00	0.00	37.69	0.00	5.88	3.25	97.27	8.38	30.16	1.89	953	0.595
Ferro-ferri-nybøite	^{W}(OH,F,Cl)	Na	$NaNa2(Fe2+3Fe3+2)(Si7Al)O22(OH)2$	43.91	0.00	5.32	37.51	0.00	0.00	9.71	96.45	16.67	22.50	1.88	958	0.597
Arfvedsonite	^{W}(OH,F,Cl)	Na	$NaNa_2(Fe^{2+}{}_4Fe^{3+})Si_8O_{22}(OH)_2$	50.13	0.00	0.00	37.46	0.00	0.00	9.70	97.29	8.33	29.97	1.88	959	0.597
oxo Ferro-pargasite	^{W}O	Ca	$NaCa_2(Fe^{2+}{}_2Fe^{3+}{}_2Al)(Si_6Al_2)O_{22}O_2$	37.55	0.00	15.93	29.94	0.00	11.68	3.23	98.33	16.63	14.97	0.00	960	0.600
Ferro-pargasite	^{W}(OH,F,Cl)	Ca	$NaCa_2(Fe^{2+}{}_4Al)(Si_6Al_2)O_{22}(OH)_2$	37.47	0.00	15.90	29.87	0.00	11.66	3.22	98.13	0.00	29.87	1.87	962	0.599

Table 2 Continue.

Name	Group	Sub-group	Formula	SiO_2	TiO_2	Al_2O_3	FeO_{tot}	MgO	CaO	Na_2O	Sum	Fe_2O_3	FeO	H_2O	M_r	cmpg
oxo Ferro-ferri-hornblende	^{W}O	Ca	$\square Ca_2(Fe^{2+}_2Fe^{3+}_3)(Si_7Al)O_{22}O_2$	43.50	0.00	5.27	37.15	0.00	11.60	0.00	97.52	24.77	14.86	0.00	967	0.603
oxo Ferro-cannilloite	^{W}O	Ca	$CaCa_2(Fe^{2+}_2Fe^{3+}_2Al)(Si_5Al_3)O_{22}O_2$	30.78	0.00	20.89	29.45	0.00	17.24	0.00	98.36	16.36	14.72	0.00	976	0.607
oxo Ferro-ferri-tschermakite	^{W}O	Ca	$\square Ca_2(Fe^{2+}Fe^{3+}_4)(Si_6Al_2)O_{22}O_2$	37.33	0.00	10.56	37.19	0.00	11.61	0.00	96.69	33.07	7.44	0.00	966	0.602
Ferro-ferri-tschermakite	$^{W}(OH,F,Cl)$	Ca	$\square Ca_2(Fe^{2+}_3Fe^{3+}_2)(Si_6Al_2)O_{22}(OH)_2$	37.25	0.00	10.53	37.12	0.00	11.59	0.00	96.49	16.50	22.27	1.86	968	0.601
oxo Ferro-actinolite	^{W}O	Ca	$\square Ca_2(Fe^{2+}_3Fe^{3+}_2)Si_8O_{22}O_2$	49.65	0.00	0.00	37.11	0.00	11.59	0.00	98.35	16.50	22.26	0.00	968	0.603
Ferro-ferri-hornblende	$^{W}(OH,F,Cl)$	Ca	$\square Ca_2(Fe^{2+}_4Fe^{3+})(Si_7Al)O_{22}(OH)_2$	43.41	0.00	5.26	37.07	0.00	11.57	0.00	97.32	8.24	29.66	1.86	969	0.602
Ferro-actinolite	$^{W}(OH,F,Cl)$	Ca	$\square Ca_2Fe^{2+}_5Si_8O_{22}(OH)_2$	49.55	0.00	0.00	37.03	0.00	11.56	0.00	98.14	0.00	37.03	1.86	970	0.602
Ferro-ferri-taramite	$^{W}(OH,F,Cl)$	Na-Ca	$Na(NaCa)(Fe^{2+}_3Fe^{3+}_2)(Si_6Al_2)O_{22}(OH)_2$	37.02	0.00	10.47	36.89	0.00	5.76	6.36	96.51	16.40	22.13	1.85	974	0.604
Ferro-ferri-katophorite	$^{W}(OH,F,Cl)$	Na-Ca	$Na(NaCa)(Fe^{2+}_4Fe^{3+})(Si_7Al)O_{22}(OH)_2$	43.14	0.00	5.23	36.85	0.00	5.75	6.36	97.33	8.19	29.48	1.85	975	0.604
Ferro-richterite	$^{W}(OH,F,Cl)$	Na-Ca	$Na(NaCa)Fe^{2+}_5Si8O_{22}(OH)_2$	49.25	0.00	0.00	36.81	0.00	5.75	6.35	98.15	0.00	36.81	1.85	976	0.604
Ferro-cannilloite	$^{W}(OH,F,Cl)$	Ca	$CaCa_2(Fe^{2+}_4Al)(Si_5Al_3)O_{22}(OH)_2$	30.72	0.00	20.85	29.39	0.00	17.20	0.00	98.16	0.00	29.39	1.84	978	0.605
oxo Ferro-rootname 4	^{W}O	Ca	$NaCa_2(Fe^{2+}_2Fe^{3+}_2Ti)(Si_5Al_3)O_{22}O_2$	30.66	8.15	15.61	29.33	0.00	11.45	3.16	98.37	16.30	14.67	0.00	980	0.608
Ferro-ferri-kaersutite	^{W}O	-	$NaCa_2(Fe^{2+}_3TiFe^{3+})(Si_6Al_2)O_{22}O_2$	36.75	8.14	10.40	29.30	0.00	11.43	3.16	99.18	8.14	21.97	0.00	981	0.609
Ferro-rootname 4	$^{W}(OH,F,Cl)$	Ca	$NaCa_2(Fe^{2+}_4Ti)(Si_5Al_3)O_{22}(OH)_2$	30.60	8.13	15.58	29.27	0.00	11.42	3.16	98.17	0.00	29.27	1.83	982	0.607
oxo Ferro-ferri-sadanagaite	^{W}O	Ca	$NaCa_2(Fe^{2+}Fe^{3+}_4)(Si_5Al_3)O_{22}O_2$	30.42	0.00	15.48	36.37	0.00	11.35	3.14	96.76	32.33	7.27	0.00	988	0.611
oxo Hastingsite	^{W}O	Ca	$NaCa_2(Fe^{2+}_2Fe^{3+}_3)(Si_6Al_2)O_{22}O_2$	36.46	0.00	10.31	36.33	0.00	11.34	3.13	97.57	24.22	14.53	0.00	989	0.612
Ferro-ferri-sadanagaite	$^{W}(OH,F,Cl)$	Ca	$NaCa_2(Fe^{2+}_3Fe^{3+}_2)(Si_5Al_3)O_{22}(OH)_2$	30.35	0.00	15.45	36.29	0.00	11.33	3.13	96.56	16.13	21.78	1.82	990	0.610
oxo Ferro-edenite	^{W}O	Ca	$NaCa_2(Fe^{2+}_3Fe^{3+}_2)(Si_7Al)O_{22}O_2$	42.49	0.00	5.15	36.29	0.00	11.33	3.13	98.38	16.13	21.77	0.00	990	0.612
Hastingsite	$^{W}(OH,F,Cl)$	Ca	$NaCa_2(Fe^{2+}_4Fe^{3+})(Si_6Al_2)O_{22}(OH)_2$	36.38	0.00	10.29	36.25	0.00	11.32	3.13	97.37	8.06	29.00	1.82	991	0.610
Ferro-edenite	$^{W}(OH,F,Cl)$	Ca	$NaCa_2Fe^{2+}_5(Si_7Al)O_{22}(OH)_2$	42.40	0.00	5.14	36.21	0.00	11.31	3.12	98.18	0.00	36.21	1.82	992	0.611
Grunerite	$^{W}(OH,F,Cl)$	Mg-Fe-Mn	$\square Fe^{2+}_2Fe^{2+}_5Si_8O_{22}(OH)_2$	47.99	0.00	0.00	50.21	0.00	0.00	0.00	98.20	0.00	50.21	1.80	1002	0.615
oxo Ferro-ferri-cannilloite	^{W}O	Ca	$CaCa_2(Fe^{2+}_2Fe^{3+}_3)(Si_5Al_3)O_{22}O_2$	29.90	0.00	15.22	35.75	0.00	16.74	0.00	97.61	23.84	14.30	0.00	1005	0.618
Ferro-ferri-cannilloite	$^{W}(OH,F,Cl)$	Ca	$CaCa_2(Fe^{2+}_4Fe^{3+})(Si_5Al_3)O_{22}(OH)_2$	29.84	0.00	15.19	35.68	0.00	16.71	0.00	97.42	7.93	28.54	1.79	1007	0.617

Table 3

Amphibole parameter	Calibration high-quality data N = 114		Test lower-quality data N = 51	
	σ_{est}	max error	σ_{est}	max error
^{T}Si	0.017	0.068	0.026	0.081
^{C}Al	0.019	0.065	0.023	0.066
^{C}Ti	0.012	0.087	0.007	0.039
Fe_T	0.007	0.045	0.024	0.121
Mg_T	0.008	0.028	0.015	0.045
Ca_T	0.005	0.019	0.005	0.016
^{B}Na	0.036	0.159	0.036	0.095
^{A}Na	0.038	0.165	0.040	0.101
^{A}K	0.002	0.007	0.002	0.005
$^{A}(Ca + Na + K)$	0.042	0.168	0.044	0.124
F	0.004	0.016	0.013	0.060
ΔMM%	0.18	0.74	0.29	0.87

N: sample number; σ_{est}: standard error of the estimate; max error: maximum error